Chapter 1

Introduction

1.1 Nanotechnology, Nanomaterial and Nanoarchitectures

Recently, Nanotechnology is growing in many areas e.g. electronics, optoelectronics, sensing and so on in the twenty-first century. Nanomaterials have structured components with at least one dimension less than 100 nm. Thus their nano dimension is in range of Debroglie wavelength. Nanostructures refer a connection between molecule and infinite bulk system. Physical and chemical properties of these nanostructures are different from the bulk material having same chemical composition. These differences between nanostructures and their bulk counterparts are related to spatial structure, shapes, electronic configuration, and chemical reactivity, catalytic and optical properties. These nanostructures can be described as following **[1-2]**.

a) Zero dimensional (0D)- Quantum dot
b) One dimensional (1D) - Nanorods, nanowires, nanotubes, nanofibers etc.
c) Two dimensional (2D) – Quantum well, sheet like structures

When all three dimensions of a bulk material are reduced to nanorange then Quantum dot formation occurs in which electrons are confined in all three dimensions. This Quantum dot is a Zero dimensional structure. On other hand if only one dimension is in nano range and electrons are confined only in one dimension then it is call Quantum well. 1D nanostructures are those materials in which electrons are confined in two dimensions because one dimension is as bulk material and two dimensions are in nanorange. Thus nanorods, nanowires, nanotubes, nanofibers are one dimensional structures.

Thus it is obvious that quantum confinement of electrons by potential wall of nanosize structures provides a powerful mean to control the electrical, optical, magnetic properties of solid state function material. The chemistry of nanostructures, energetic, response, dynamics, and uniqueness of the structural characteristics constitutes the basis of nanoscience. Table 1.1 lists the typical dimensions of nanomaterials **[3]**.

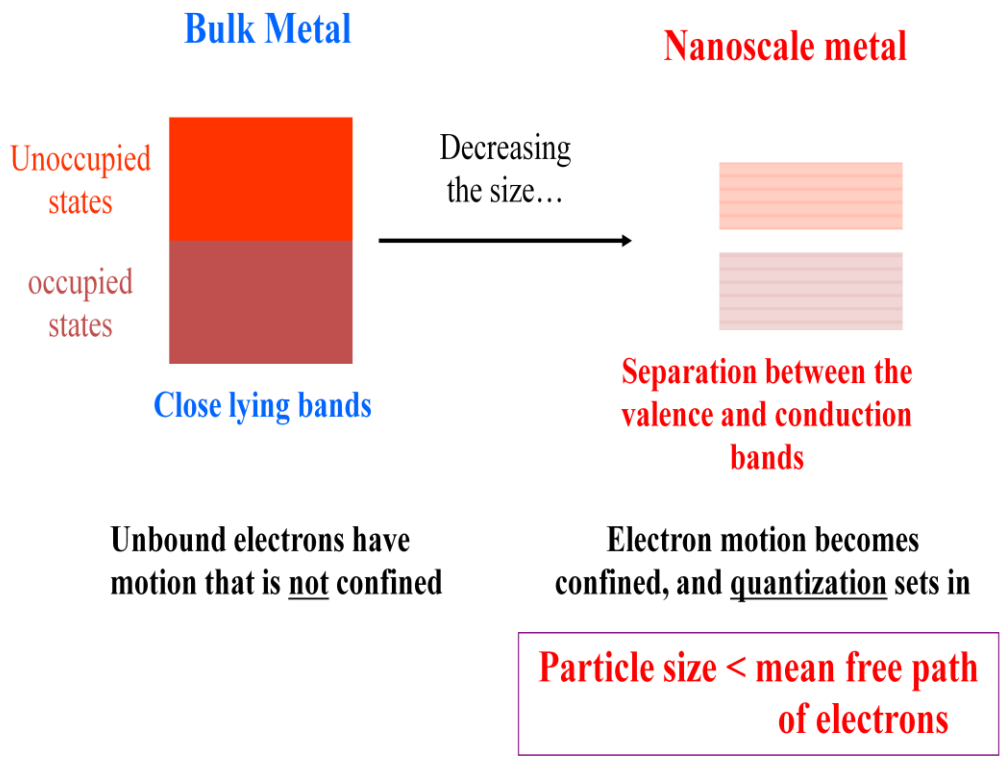

Fig 1.1 Comparison between nanomaterials and their bulk counterparts **[3]**

Most essential aspect of nanomaterials is their size effect. When bulk material is reduce to nano dimension then no of electron at the surface of structures increases drastically which leads to increment of surface area to volume ratio of material.

$$\text{Specific surface area} = \frac{4\pi r^2}{\frac{4}{3}\pi r^3 \rho} = \frac{3}{\rho r}$$

Where r is radius of nanoparticles and ρ is its density. Thus Surface area of a nanomaterial per unit volume depends on its radius. This increase surface to volume ratio results in highly modified reaction time and catalytic behavior.

The density of states (DOS) varies according to different type of nanostructures depending upon their electron confinement as shown in fig 1.2. In case of bulk material the DOS (number of electronic states per unit volume and energy) depends on square root of its energy. This dependence changes according to quantum confinement. The variation in DOS with

dimensionality results in outstanding electrical and optical properties for realizing advanced nanodevices.

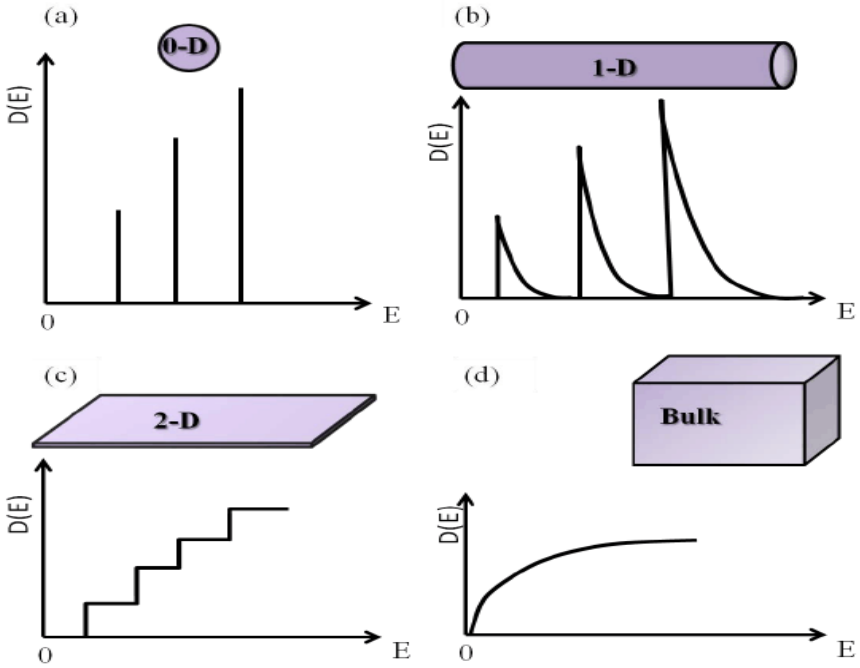

Fig 1.2 Schematic representation of the DOS : (a) 0-dimension (0-D), (b) 1-dimension (1-D), (c) 2-dimension (2-D) and (d) 3-dimension(3-D) **[4]**

Nanostructure	Size	Material
Clusters, nanocrystals quantum dots	Radius, 1-10 nm	Insulators, semiconductors, metals, magnetic materials
Other nanoparticles (NPs)	Radius, 1-100 nm	Ceramic oxides
Nanobiomaterials, Photosynthetic reaction center	Radius, 5-10 nm	Membrane protein
Nano Wires	Diameter, 1-100 nm	Metals, semiconductors, oxides, sulfides, nitrides
Nanotubes	Diameter, 1-100 nm	Carbon, layered Chalcogenides, BN, GaN
Nanobiorods	Diameter, 5 nm	DNA
Two-dimensional (2D) arrays of NPs	Area, several nm^2- μ m^2	Metals, semiconductors, magnetic materials

Table 1.1 Nanostructures and their assemblies **[3]**

1.2 History

Although technology may be a comparatively recent development in research, the event of its central ideas happened over an extended amount of your time. In 1974, Norio Taniguchi introduced the term "Nanotechnology" to represent additional – high exactness and extremist – fine dimensions, and additionally foretold enhancements in integrated circuits, optoelectronic devices and store devices. The emergence of technology within the Eighties was caused by the convergence of experimental advances like the invention of the scanning tunneling magnifier in 1981 and therefore the discovery of fullerenes in 1985. The scanning tunneling magnifier, Associate in nursing instrument for imaging surfaces at the atomic level, was developed in 1981 by Gerd Binning and Heinrich Rohrer at IBM city work, that they received the Nobel Prize in Physics in 1986. Fullerenes were discovered in 1985 by Harry Sir Harold Walter Kroto, Richard Errett Smalley, and Robert Floyd Curl Jr., UN agency along won the 1996 Nobel Prize in Chemistry.

Around the same time, K. Eric Drexler developed and popularized the construct of technology and supported the sector of Molecular technology. In 1979, Drexler encountered Richard Feynman's 1959 speak "There's many space at the Bottom" **[35]**. The term "nanotechnology", originally coined by Norio Taniguchi in 1974, was inadvertently taken by the Drexler in his 1986 book "Engines of Creation: the approaching Ero Nanotechnology"**[36]**, that planned the concept of a nanoscale "assembler" which might be ready to build a replica of itself and of different things of discretional complexness. Drexler's vision of technology is commonly known as "Molecular Nanotechnology" (MNT) or "molecular producing," and Drexler at one purpose planned the term "zettatech" that never became in style.

In the early 2000s, the sector was subject to growing public awareness and contention, with outstanding debates concerning each its potential implications, exemplified by the Royal Society's report on technology, further because the feasibleness of the applications unreal by advocates of molecular technology, that culminated within the public speaking between Eric Drexler and Richard Errett Smalley in 2001 and 2003. Several nations affected to push and fund analysis into technology with programs like National technology Initiative, Centre for technology. The first 2000s additionally saw the beginnings of economic applications of technology, though these were restricted to bulk applications of nanomaterials, like the Silver, Nano platform for victimization Silver Nano platform for victimization silver nanoparticles as an

antibacterial drug agent, nanoparticles-based clear sunscreens, and carbon nanotubes for stain-resistant textiles.

According to Dr. K. Eric Drexler there are some units that become sensible with mature nano engineering science **[35]**.

- Nearly free client merchandise
- PCs billions of times quicker than nowadays
- Safe and cheap spaceflight
- Virtual finish to unhealthiness, aging, death
- No a lot of pollution and automatic cleanup of existing pollution
- End of famine and starvation
- Reintroduction of the many extinct plants and animals.

Properties of the solids are unit obsessed to their size. The properties of the majority materials are largely preserved until the reduction of their dimensions in micrometer vary. However, the size of materials is reduced to nanomaterials. As an example, take into account the case of nano gold particles , it doesn't show characteristic yellow color at this scale however show completely different colors, orange, red, purple or chromatic relying upon the particular size of the particles. Compared to bulk, the temperature and chemical properties conjointly modify once the fabric is reduced to nanoform. The melting temperature of nano type reduces considerably. Bulk semiconductors become insulators once dimensions are reduced to nanometers. The first cause for the forceful modification in behavior of nanomaterials compared to their bulk type is that in nano range the quantity of atoms on the surface could be a huge fraction of the overall number of atoms within the material i.e. giant surface to volume quantitative relation.

1.3 One dimensional (1D) - Nanorods, nanowires, nanotubes, nanofibers etc

Nanorods, nanowires, nanotubes, nanofibers etc are one dimensional structure because in those materials electrons are free to move only in one dimension along the axis and confined in other two dimensions which creates drastic change in electrical, optical, magnetic and thermal behavior of a bulk material. These 1D structures are used for tunneling of electrons from one potential wall to other. The properties of Nanorods are very much different from those at a larger

scale. The properties of Nano Materials get existence due to two principal factors to differ significantly from other materials.

1. Quantum confinement effect.
2. Increased surface area to volume ratio.

These factors can charge or enhance properties such as reactivity, strength and electrical characteristics. These 1D nanomaterials can be formed by semiconductor or metals by various synthesis techniques.

In this thesis I have reported Metal oxide Nanorod, nanowires and nanoflowers. Some metal oxides behave as a semiconductor because of their moderate bandgap. Metal oxide materials can be classified as following **[4].**

- Transitional metal oxides (Fe_2O_3, NiO, Cr_2O_3, etc.)
- Non transitional metal oxide
  - Post transitional (Al_2O_3, etc.)
  - Pre transitional (ZnO, SnO_2 and CuO etc.)

Recently, much attention has been paid to nanocrystalline semiconductor structures because of having considerable interest in their properties such as unique optical properties, increased activity, large surface to volume ratio and special electronic properties compared to those of bulk materials **[5].** The oxides of transitional metals are an important class of semiconductors. Among these, Copper oxide (CuO), as a p-type transition-metal-oxide semiconductor with narrow band gap of 1.2 eV **[6,7]** with excellent applications in Li-ion batteries, solar cells, gas sensors, Bio sensors, Field Emission Emitter etc., has attracted much attention among researchers all over the world **[8-13]**. Various methods like thermal oxidation of copper foil, hydrothermal route, aqueous reaction, vapor-liquid-solid synthesis, solution-liquid-solid synthesis, laser ablation, arc discharge, precursor thermal decomposition, electron beam lithography, and template-assisted synthesis, etc. **[14-19]** have been employed for fabrication of well aligned nanostructures.

However, it is still a challenging task to synthesize a simple and suitable method for large scale synthesis of nanostructured CuO with a designable morphology. These methods require high temperature, complex instrumentation, and inert atmosphere and are costly for large scale production. Thus simple and cost effective methods are needed for these nanoarrays **[20]**. In this work, wet chemical method has been used for synthesis of CuO nanorods. This method is

comparatively simple and cost effective which can be performed at room temperature in ambient atmosphere. The structural and morphological properties of copper oxide nanostructures were thoroughly investigated and characterized along with suitable growth mechanism.

1.4 Metal oxide nanostructures

In the field of metal oxides, the invention of superconductive oxides and oxides with giant magneto resistance **[37]** has raised special attention particularly to oxides with transition metals (Figure 1.3) **[38].** Transition metal oxides are usually used as catalysts and in physical science with applications varied from semiconductors, dielectrics and semi conductive electrodes, which suggest the importance of those materials **[39].** Metal oxides have the benefit of the big tendency of the element to induce sturdy lepton connections with the close atoms that affects the chemical properties and surface energy of the materials **[40].** At constant time, nanostructured metal oxides compared with the majority materials have the benefit of the abstraction confinement at the side of the large fraction of surface atoms, high surface energy, robust surface sorption and magnified surface to volume quantitative relation that greatly improves the performance of those materials. The variation of electronic structures in oxides is sort of wide, wherever transition and post-transition metal oxides show terribly attention-grabbing properties.

Transition metal oxides are characterized by a small energy distinction between cation d_n and either d_{n+1} or d_{n-1} configurations, that permits to fast transformation between the various forms. However, the structure instability and non optimality of different parameters will limit the fields of application. Solely metal oxides with d_0 and d_{10} electronic configurations show stable properties. The d_0 configuration is found in transition-metal oxides, such as, CuO, TiO_2, V_2O_5 and WO_3, whereas d_{10} configuration is found in post-transition-metal oxides, as In_2O_3 or SnO_2.

The deposition of nanostructured metal oxides has been already delineated by each physical and chemical ways and it's believed that each one the understanding relating to the synthesis, properties and applications of nanoparticles, delineated antecedently, may also be extended to compounded nanoparticles.

H																	He
Li	Be											B	C	N	O	F	Ne
Na	Mg											Al	Si	P	S	Cl	Ar
K	Ca	Sc	Ti	V	Cr	Mn	Fe	Co	Ni	Cu	Zn	Ga	Ge	As	Se	Br	Kr
Rb	Sr	Y	Zr	Nb	Mo	Tc	Ru	Rh	Pd	Ag	Cd	In	Sn	Sb	Te	I	Xe
Cs	Ba	La	Hf	Ta	W	Re	Os	Ir	Pt	Au	Hg	Tl	Pb	Bi	Po	At	Rn
Fr	Ra	Ac	Rf	Db	Sg	Bh	Hs	Mt	Ds	Rg	Cn		Fl		Lv		

Transition metals

Post-transition metals

Fig 1.3 Transition and post-transition metals teams highlighted within the tabular array **[42]**

1.5 Properties of copper oxide

Copper oxide is of great interest in semiconductor physics among other compound semiconductors. Copper reacts with oxygen and forms two stable metal oxide semiconductors. First one is cupric oxide (CuO) and other one is cuprous oxide (Cu_2O) having different colors, different physical properties, electrical properties and crystal structures. CuO is chosen for sensing applications because of its interesting properties like monoclinic structure, nonhazardous source materials and it can be prepared by low cost solution methods which are required for gas sensing applications. **Figure 1.4** shows the monoclinic structure of the CuO.

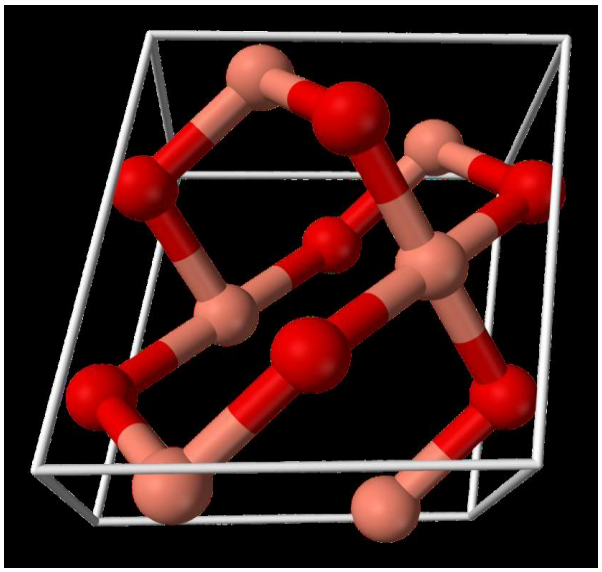

Fig 1.4 Copper (II) oxide (CuO) crystal structure **[23]**

Property	Value	Reference
Lattice constants (300K)	a = 4.68 Å b = 3.42 Å c = 5.13 Å	[28, 26]
Density	6.31 gm/cm^3	[24]
Melting point	1975 ^{o}C	[24]
Stable phase at 300 K	Monoclinic	[26]
Dielectric constant	18.1	[24]
Refractive index	1.4	[24]
Band gap (Eg)	1.21-1.55 eV direct	[27]
Hole effective mass	0. 24 m_o	[28]
Hole mobility	0.1-10 cm^2/V s	[24]

Table 1.2 Key properties of CuO at room temperature (300 K) **[23]**

CuO is a p type semiconductor material having bandgap1.21-1.55 eV and monocline stable phase structure. This CuO material is useful due to high melting point of 1975 ^{o}C and density 6.31 gm/cm^3. Nanostructures of CuO are used in many applications of various fields.

1.6 Application of various CuO nanomaterials

CuO nanomaterials have drastically modified properties over their bulk counterparts because of their high surface to volume ratio. Due to this property CuO nanorods and nanowires have many promising application in many fields. These applications can be described as below.

i. CuO nanomaterials used as Li-ion batteries
ii. CuO nanomaterials used as Dye sensitized solar cells
iii. CuO nanomaterials used as gas sensors
iv. CuO nanomaterials used as bio sensors
v. CuO nanomaterials used as field emission emitter

vi. CuO nanomaterials used as Super capacitor

vii. CuO nanomaterials used as Lithium storage application

viii. CuO nanomaterials used as Uric acid biosensor

ix. CuO nanomaterials used as Glucose Biosensor

1.6.1 CuO nanomaterials used as Li-ion batteries

X. P. Gao, J. L. Bao and other scholars have shown the use of CuO nanorods in Li ion batteries. In Li-ion batteries CuO nanorods can be act as an anode material which exhibits a high electrochemical capacity of 766 mAh/g and relatively poor capacity retention as compared to thick single crystalline nanorods. Whereas a bulk single crystalline material have electrochemical capacity 416 mAh/g only that's why CuO nanorods are preferred over these bulk material. A new fuel cell material with enhanced performance has been developed with CuO nanorods as anode material and spinel $LiNi_{0.5}Mn_{1.5}O_4$ as cathode. The full cell exhibits capacity retention of 84% at 0.5C over 100 cycles and a discharge capacity of 240 mAh g^{-1} at a high rate of 10C **[29]**.

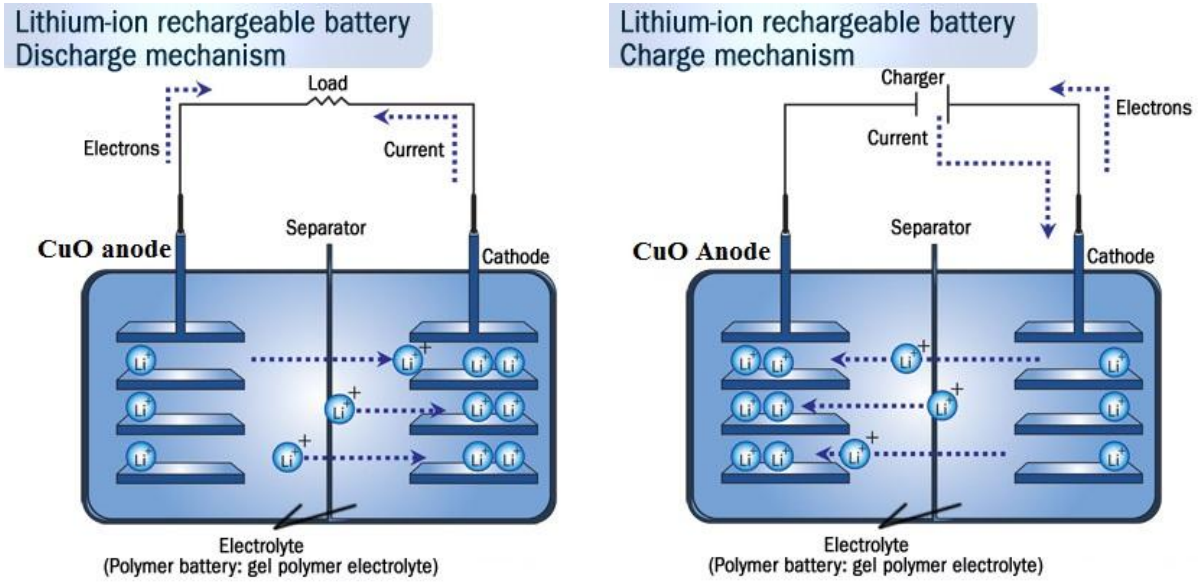

Fig 1.5 Schematic showing Charging and discharging of Li Ion batteries, having CuO nanoarrays as anode material **[29]**

1.6.2 CuO nanomaterials used as Dye sensitized solar cells

Cuo nanorods have promising application in dye sensitized solar cell. These CuO nanorods are used as hole transport media for solar energy conversion in hetero junction of Dye sensitized solar cells. The CuO nanorods/Cu electrode has been used as a cathode in dye-sensitized solar cells based on n-TiO2 nanoparticles having overall energy conversion efficiency up to 0.29% **[30]**.

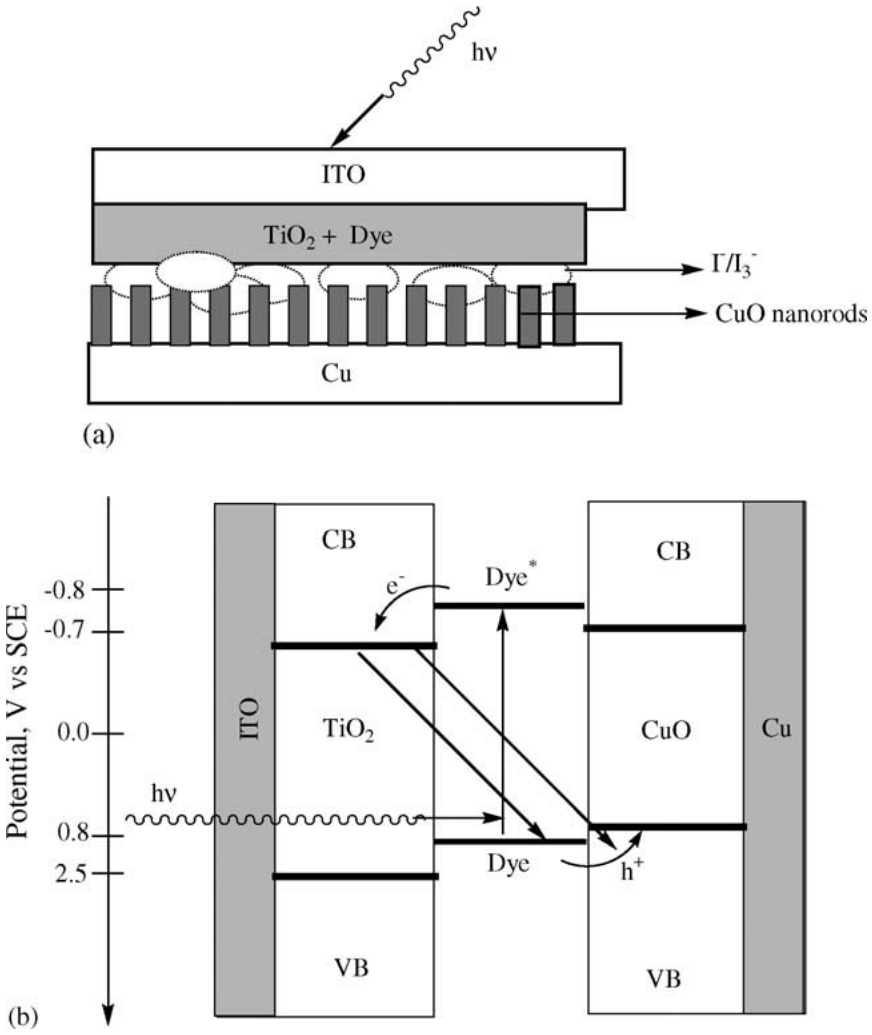

Fig 1.6 (a) Schematic illustration of the dye-sensitized photovoltaic cell having CuO nanorod as anode material (b) Schematic energy level diagram showing the band structure alignment and photo induced charge separation in the photovoltaic cell in (a) (the energy level positions are approximate) **[30]**.

1.6.3 CuO nanomaterials used as gas sensors

CuO nanomaterials can be used as gas sensing material because of their enhanced surface to volume ratio. Due to enhanced surface to volume ratio physiosorption and chemisorptions on the surface of CuO increase and catalytic properties also enhance which result in to variation of material resistance which can be detected and gas sensing occur. As prepared CuO gas sensor shows high response to ethanol at low temperature and having less recovery time. This CuO based sensor can be used to sense many other gases like xylene, acetone, toluene and cyclo-hexane. The response of the CuO sensor to ethanol (1000 ppm) is 9.8 at the working temperature of 210 ˚C. The response time and the recovery time are within the range of 13–42 s and 17–51 s **[31]**.

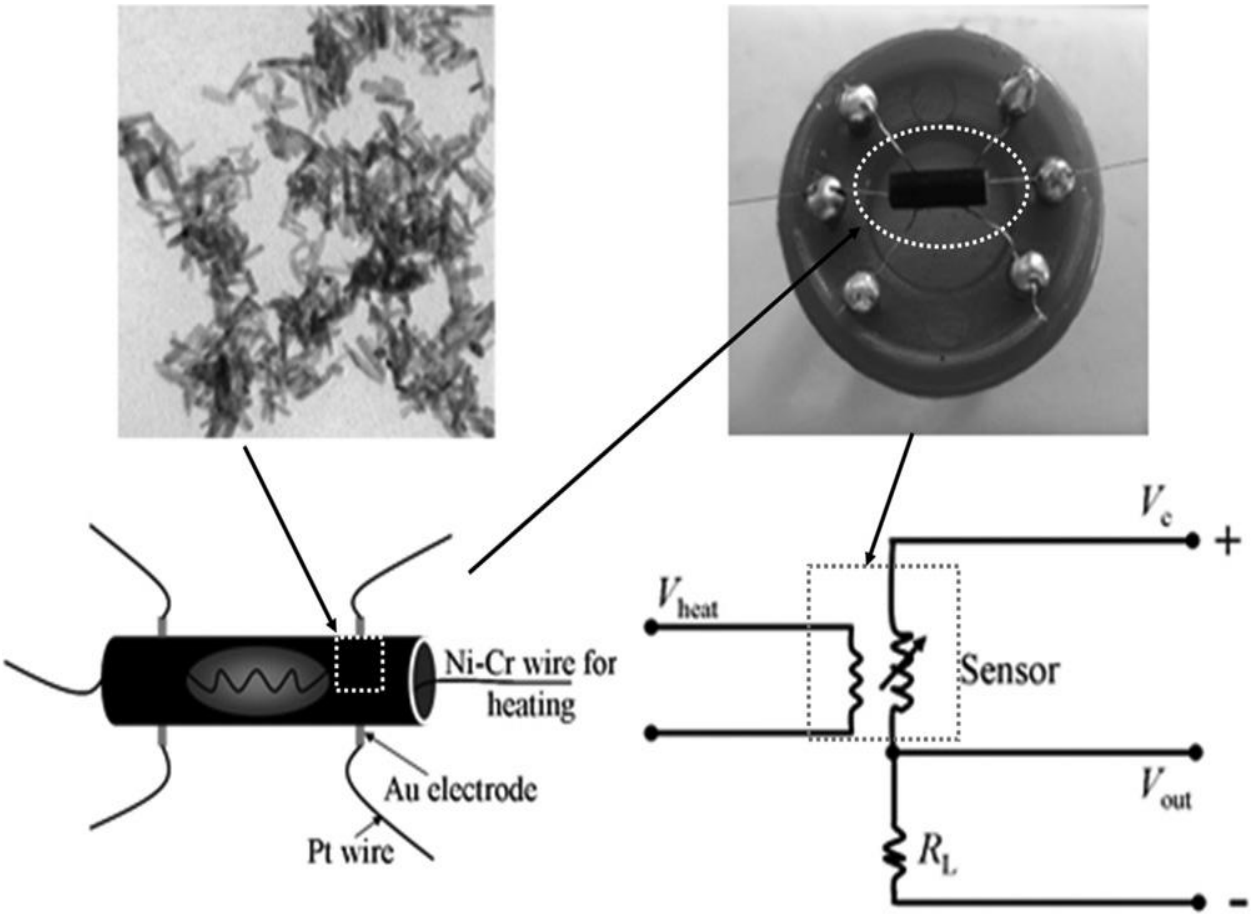

Fig 1.7 Schematic illustration of fabrication of the gas sensor using CuO nanorods as sensing material **[31]**

1.6.4 CuO nanomaterials used as bio sensors

The CuO NPs were developed as an ink using mixed solvents of ethanol, iso-propanol, water and diethylene glycol with twenty wt% CuO NPs. As-formulated ink sample was utilized to fabricate a brand new Glucose biosensor supported inkjet written Si/Ag/CuO NPs conductor. It is observed that microwave-assisted tempering produces sleek surface with interconnected third-dimensional nanofilms on Ag/Si electrode with none structural defects. The invented detector presents variety of engaging analytical options like high sensitivity, sensible stability, duplicability, property, and wide linear vary still as quick interval. The information from biosensor determination in blood serum samples are unit in accordance with the calculated ones. This inkjet printing technique will simply be used for the mass-production of electrodes victimization CuO NPs-ink not solely on the Si/Ag conductor however additionally on the variability of electrodes material to use for long as associate amperometric sensor for routine analysis of aldohexose in real blood samples still as in agricultural merchandise or foods **[32]**.

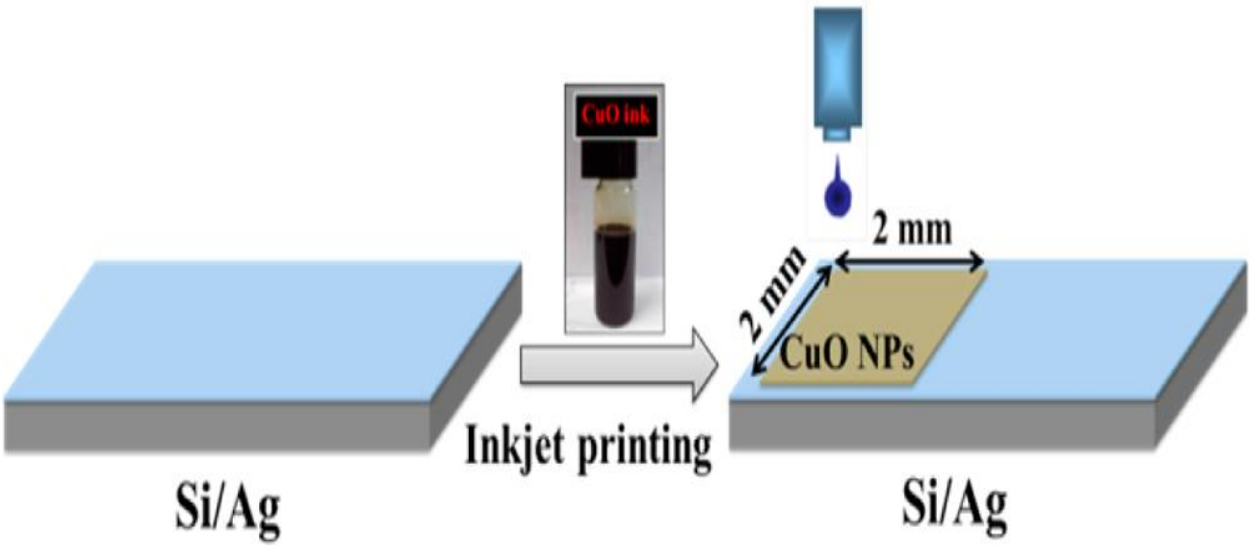

Fig 1.8 Schematic illustration of CuO NPs used in bio sensors fabricated by ink jet printing **[32]**

1.6.5 CuO nanomaterials used as Super capacitor

CuO nanomaterials can be used as an active material for a capacitor. Voltammograms square measure constant in form except within the current intensities of the oxidation-reduction peaks comparable to quasi-reversible transition between +2 and +1 oxidization state of CuO. Throughout this method, CuO converts into Cu_2O by dynamical its number from +2 to +1 and contrariwise. The precise capacitance of the active material is calculated from the charge transferred through the forward and backward scans that is equal to the realm below the curves. the precise capacitance can then be calculated victimisation the subsequent equation **[33]**.

$$C_{sp} = \frac{\bar{I}}{m\nu}$$

Where C_{sp} is that the specific capacitance (F g^{-1}), I is the average current (A), m is that the mass of active material (g) (CuO scraped from copper foil), and ν is that the potential scan rate (V s^{-1}). This ends up in a lot of interfacial surface between the nanostructures and also the electrolyte, resulting in a lot of fascinated reactions. Thus morphology of CuO nanomaterials can affect the pseudo-capacitive performance of CuO.

1.6.6 CuO nanomaterials used as field emission emitter

The field emission of a CuO nanoneedle possesses smart field-emission properties, such as low stimulation field of 5.3 V/μm, high most current of 1.08 μA at 9.7 V/μm, and linear F–N graph, indicating that the present CuO nanoneedle would be an honest potential application in field-emission space. 2 completely different slopes appear within the corresponding F–N graph, that represents that the work perform of this CuO nanoneedle is to be 1.12 and 0.58 work unit at high- and low-field regions, respectively. At an equivalent time, the sector increasing β of the CuO nanoneedle's film is calculated to be 769 and 661, and their corresponding parameter s for screening impact is 0.1153 and 0.0989, severally. This showed that the screening impact compete a key role within the field-emission properties **[34]**.

Chapter 2

2.1 Preferential methods adopted for the synthesis of CuO nanostructures

CuO nanostructures can be synthesized by various methods depending upon their morphology. In this concern various methods like thermal oxidation of copper foil, hydrothermal route, aqueous reaction, vapor-liquid-solid synthesis, solution-liquid-solid synthesis, laser ablation, arc discharge, precursor thermal decomposition, electron beam lithography, and template-assisted synthesis, etc. can be discussed. But many of them require high synthesis cost, perfect ambient condition, high temperature, highly précised equipments which causes high attention and cautiousness. Among these methods wet chemical method is simple and cost effective which can be occurred at normal temperature and pressure.

2.1.1 Synthesis of copper oxide nanoparticles by solution plasma

Genki Saito, Sou Hosokai describes the synthesis of copper/copper chemical compound nanoparticles via solution plasma, in which the result of the solution and electrolysis time on the morphology of the product was mainly examined. Within the experiments, a cathode of copper wire was immersed in associate in nursing electrolysis solution of a K_2CO_3 with the concentration variation from 0.001 to 0.50 M and was melted by the local-concentration of current. The results incontestable that by victimisation the K_2CO_3 solution, we have a tendency to obtained CuO nanoflowers with several sharp nanorods, the scale of that decreased with decreasing the concentration of the solution. Spherical particles of copper with/ without pores shaped once the citrate buffer was used. The pores within the copper nanoparticles appeared once the applied voltage modified from one hundred five Volts to one hundred thirty Volts, owing to the dissolution of Cu_2O **[43]**.

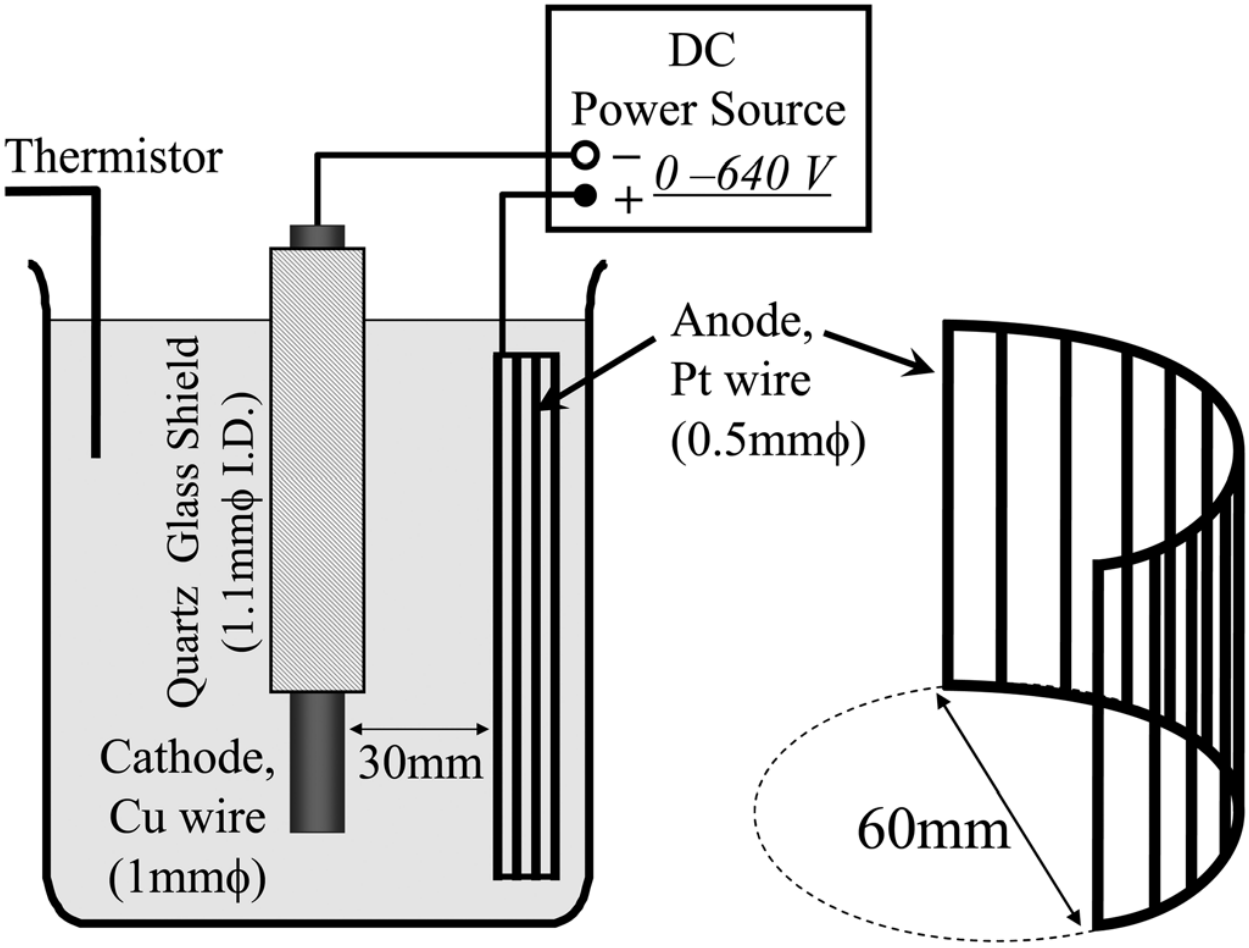

Fig 2.1 Schematic diagram of instrumental setup for synthesis of CuO nanostructures **[43]**

2.1.2 Synthesis of copper oxide nanoparticles by laser ablation

X. Z. Lin, P. Liu, J. M. Yu have synthesized CuO nanostructures via laser ablation method for controlled and précis growth of nanoarchitectures. They described a unique nanomanufacturing, which may bring home the bacon from nanocrystal synthesis to successive purposeful structure nanomanufacturing inside one step. This novel technique is that the electrical field assisted optical laser ablation in liquid (EFLAL). Exploitation EFLAL, they have a tendency to 1st synthesize CuO nanocrystals and consecutive fabricate CuO functional structures, i.e., nanospindles with shape-dependent optical absorption that are expected to be applicable to biology or medication. Significantly, these two processes, synthesis and assembly, are finished within one step.

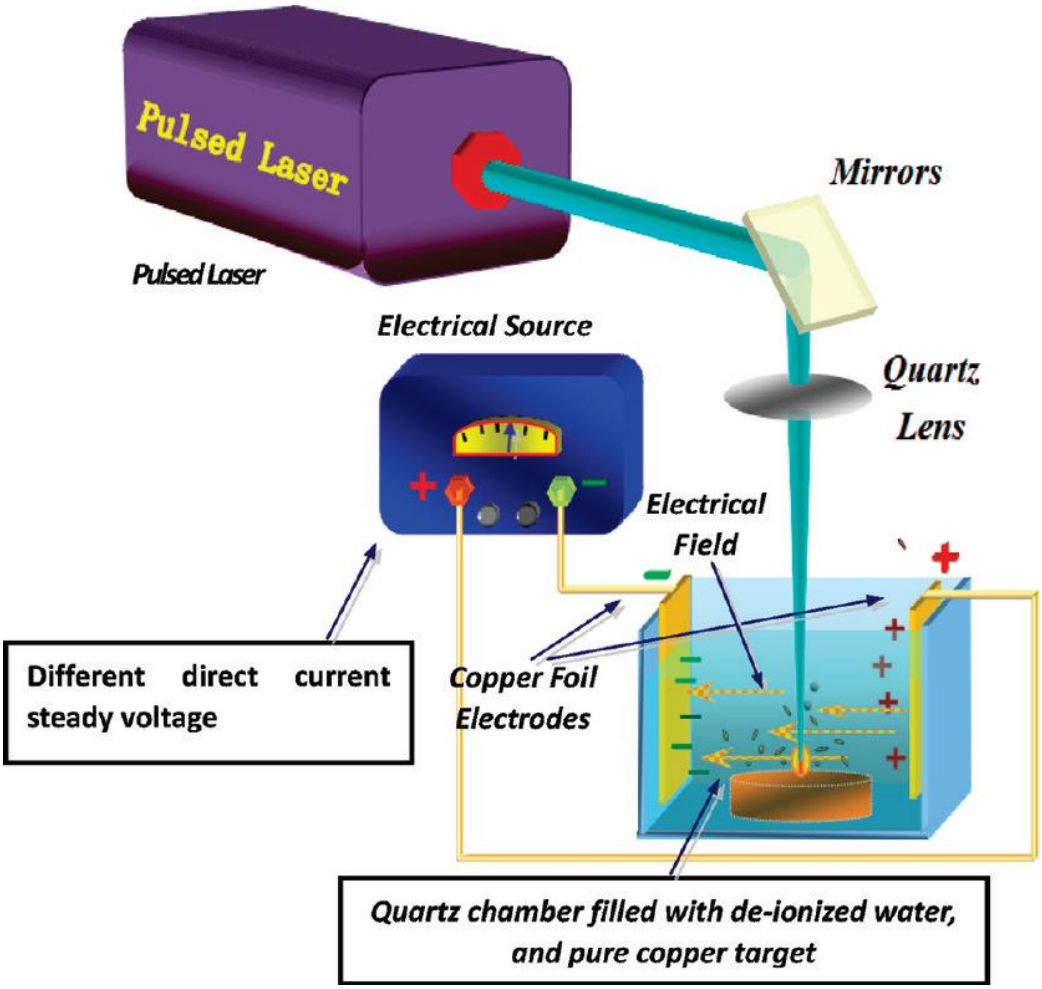

Fig 2.2 Schematic diagram of laser ablation setup for synthesis of CuO nanostructures **[44]**

Firstly, the second harmonic is produced by a Q-switch neodymium-doped yttrium aluminum garnet laser device with a wavelength of 532 nm, pulse breadth of ten ns continuance frequency of five Hz, and pulse energy of 100 mJ/pulse. Next, the one copper target with 99.7% purity is employed because the beginning material and is mounted on all-time low of the oblong quartz chamber, and deionized water is poured slowly into the chamber till the target is covered by concerning ten millimeter. Then 2 copper foil electrodes with 99.99% purity are mounted against the walls of the chamber as shown in figure. The distance between the 2 electrodes is about forty eight millimeter. The DC electrical field with adjusting voltage is produced by an immediate current steady voltage power supply. Finally, the heartbeat optical device is targeted on the surface of the target. During optical device ablation, completely different voltages (V)

(zero, 40, 80, and 120 V) are applied, and therefore the target and solution are maintained at temperature. When the laser device interacted with the target for sixty min, the yellow solution is collected before additional measurements. Significantly, these 2 processes, synthesis and assembly, are finished within one step **[44]**.

2.1.3 Synthesis of copper oxide nanoparticles by thermal decomposition on silicon substrate

Large-area and aligned oxide nanowires are synthesized by thermal tempering of copper thin films deposited onto semiconductor substrate. The effects of the film deposition methodology, hardening temperature, film thickness, annealing gas, and patterning by lithography are consistently investigated. Long and aligned nanowires has been shaped inside a narrow temperature vary from 400-500 ˚C. Electroplated copper film is favorable for the nanowire growth, compared to it deposited by thermal evaporation. Hardening copper thin film in static air produces large-area, uniform, however not well vertically aligned nanowires on the skinny film surface. Annealing copper thin film in a N_2/O_2 gas flow generates vertically aligned non uniform nanowires on massive areas. Patterning copper thin film by lithography helps to synthesize large-area, uniform, and vertically aligned nanowires on the film surface. Bicrystal CuO nanowires are converted by the copper thin film and conjointly maybe some CuO film once the thermal treatment in static air. Solely CuO within the kind of bicrystal nanowires and thin film is determined once the copper skinny film is annealed in a N_2/O_2 gas flow **[46].**

2.1.4 Synthesis of CuO nanorods by a Solid-Liquid Phase Arc Discharge Process

Uniform and monodisperse CuO nanorods are synthesized by directional aggregation and crystallization of tiny CuO nanoparticles. These nanoparticles can be generated from a solid-liquid arc discharge method below ambient conditions without any surfactants. Uniform CuO nanorods with sharp ends are shaped from little nanoparticles via fast oxidization of Cu nanostructures, the Ostwald ripening method including agglomeration of CuO nanoparticles. The spontaneous aggregation and familiarized attachment of tiny CuO nanoparticles contributed clearly to the formation of those sorts of nanostructures. Cu and Cu_2O nanoparticles are often selectively synthesized by stopping the oxidization of Cu via suitable chemical agent **[45]**.

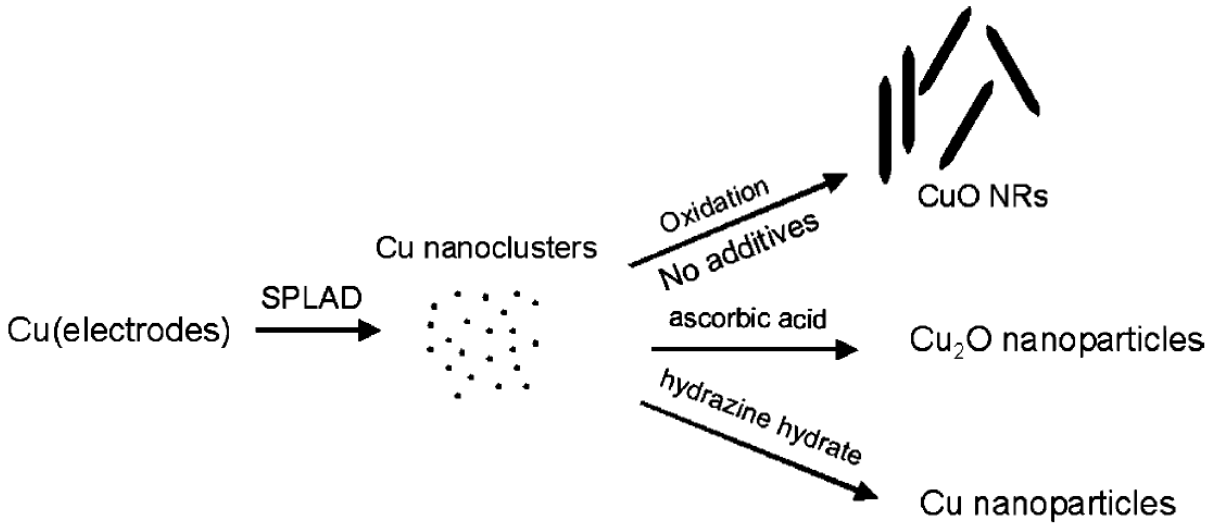

Fig 2.3 Illustration of the Selective Synthesis of CuO, Cu_2O, and Cu Nanoparticles by the SLPAD Method **[45]**

2.2 Literature survey

A literature survey forms a very important and indispensable module of a groundwork project. It throws lightweight on the number of study done to date within the chosen material, showcases the issues and gaps within the previous analysis, pinpoints the new scopes of analysis arising out of these studies, highlights the standing of analysis being applied by the modern analysis teams within the relevant field round the globe and eventually, saves time, funds and energy of a investigator from ending up in some conclusions that have already been discovered by another analysis group at some early date. Also, it prevents the analysis knowledge domain from being affected by plagiarism to a good extent.

A substantial quantity of literature review has been wiped out this project. This chapter provides an outline on the various synthesis strategies for the synthesis of CuO nanorods and architectures adopted by totally different analysis teams and their pros and cons moreover as their practicability in development. Moreover, it throws lightweight on the study applied round the globe on the properties and ways that and suggests that to tailor them as per the requirements of the semiconductor industry.

M. M. Momeni, Z. Nazari, A. Kazempour, M. Hakimiyan and S. M. Mirhoseini have coated Cu nanostructures on Cu substrate for using it as Super capacitor material. They

illustrated that the pseudo-capacitor performance of oxide is tuned via using completely different samples. They develop a simple and facile synthesis process for growth of CuO nanostructures on Cu foil at ambient temperature **[47]**.

Genki Saito, Sou Hosokai describes the synthesis of copper/copper chemical compound nanoparticles via solution plasma, in which the result of the solution and electrolysis time on the morphology of the product was mainly examined. Within the experiments, a cathode of copper wire was immersed in associate in nursing electrolysis solution of a K_2CO_3 with the concentration variation from 0.001 to 0.50 M. The results incontestable that by victimisation the K_2CO_3 solution, we have a tendency to obtain CuO nanoflowers with several sharp nanorods, the scale of that decreased with decreasing the concentration of the solution. Spherical particles of copper with/ without pores shaped once the citrate buffer was used. The pores within the copper nanoparticles appeared once the applied voltage modified from one hundred five Volts to one hundred thirty Volts, owing to the dissolution of Cu_2O **[43]**.

Wei-Tang Yao, Shu-Hong Yu, Yong Zhou have synthesized CuO nanorods by arc discharge method Uniform and monodisperse CuO nanorods are synthesized by directional aggregation and crystallization of tiny CuO nanoparticles. These nanoparticles can be generated from a solid-liquid arc discharge method below ambient conditions without any surfactants. Uniform CuO nanorods with sharp ends are shaped from little nanoparticles via fast oxidization of Cu nanostructures, the Ostwald ripening method including agglomeration of CuO nanoparticles **[45]**.

Su Yi-kun, Shen Cheng-min have used sol gel technique for synthesis of templated assited CuO nanorords. they synthesised it within a porous anodic aluminum oxide (AAO) template by a citrate-based sol-gel route. To draw the gel in template a capilary action is used through a vaccume system thus CuO nanowires are fabricated by solgel technique which is controlled growth mechanism for its synthesis **[48]**.

Sambandam Anandan, Xiaogang Wen have synthesized CuO nanorods via simple and cost effective wet chemical method at room temerature and they have used this CuO nanostructures as cathod material in dye sensitized solar cell **[49]**.

Chao Yanga, Xintai Sua have synthesised CuO nanorods by hydrothermal route which is microwave assisted. They used it for gas sensing of several organic vapors. Due to small partical

size of CuO nanostructures, the gas sensing performance of sensors enhanced for ethanol gas sensing **[50]**.

Anita Sagadevan Ethiraj and Dae Joon Kang have reported a productive synthesis of oxide nanowires with a mean diameter of ninety nm and lengths of several micrometers by employing a easy and cheap wet chemical methodology. The CuO nanowires prepared via this methodology are advantageous for industrial applications that need production and low thermal budget technique. It's found that the concentration and therefore the amount of precursors are the important factors for getting the desired one-dimensional morphology **[51]**.

X. P. Gao, J. L. Bao and other scholars have shown the use of CuO nanorods in Li ion batteries. In Li-ion batteries CuO nanorods can be act as an anode material which exhibits a high electrochemical capacity of 766 mAh/g and relatively poor capacity retention as compared to thick single crystalline nanorods. Whereas a bulk single crystalline material have electrochemical capacity 416 mAh/g only that's why CuO nanorods are preferred over these bulk material.

Rafiq Ahmad, Mohammad Vaseem have illustrated the application of CuO nanostructures as wide linear-range detecting nonenzymatic glucose biosensor. The CuO NPs were developed as an ink using mixed solvents of ethanol, iso-propanol, water and diethylene glycol with twenty wt% CuO NPs. As-formulated ink sample was utilized to fabricate a brand new Glucose biosensor supported inkjet written Si/Ag/CuO NPs conductor. It is observed that microwave-assisted tempering produces sleek surface with interconnected third-dimensional nanofilms on Ag/Si electrode with none structural defects.

R. Sathyamoorthy and K.Mageshwari have synthesized hierarchical CuO microspheres for Photocatalytic and antibacterial activities. It was synthesized by reflux condensation route. They investigated the activity of CuO nanospheres against photodegradation of methyl orange dye and antibacterial activity **[52]**.

Chapter 3

3.1 Growth mechanism

There are various growth mechanisms for synthesis of nanorods of various metals and metal oxide. Top to down and bottom up approach are used to elaborate the growth mechanism of nanorods nanowires and nanowishkers. Here two main growth mechanisms are described, which are given below.

a) Vapour liquid solid growth mechanism (VLS)
b) Ligand assisted solid liquid growth mechanism (LSS)
c) Vapour solid solid growth mechanism (VSS)

But in my work described growth mechanism is Ligand assisted solid liquid growth mechanism (LSS) which can successfully describe the growth mechanism of CuO nanorods and nanowires.

3.1.1. Vapour liquid solid growth mechanism (VLS)

The basis of all is that the vapor-liquid-solid (VLS) mechanism that was originally developed for the growth of element whiskers by Wagner and Ellis. It consists of the belief that a volatilized part, a liquid part and a solid interacts. The precursor is provided because the gas. The liquid part is liquefied molten catalyst particle exist on the solid substrate. Throughout this growth method it's ascertained that the precursor decomposed during a specific space of the surface of the liquid particle at the temperature T_1. The precursor material dissolves till saturation at concentration c1 is earned. It's assumed that this particle occupies a locality with a lower temperature T_2 and a lower concentration c_2. Therefore the presence of each a level and thermal gradient is assumed. The Precursor material diffuses through the particle and precipitates at T_2. These very basic assumptions of the mechanism enable the applying to different systems.

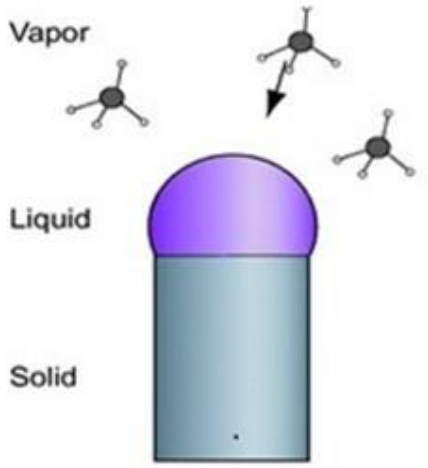

Fig 3.1 Representation of VLS mechanism **[58]**

Base and tip growth mode

This is one amongst the very initial mechanism to clarify growth of the carbon whiskers that was at the start developed by Baker on basis of VLS mechanism. He and his group performed unchanged studies on growth of the carbon whiskers by using controlled atmosphere electron microscopy (CAEM). Throughout this formation, the liquefied metal catalyst particles were either on top or bottom of as-formed whiskers. Due to the forces functioning on these catalyst particles, they undergo deformation throughout the method which ends up in 2 totally different growth modes. If there's robust attractive interaction between catalyst and substrate, then a decent wettability is found that result in the contact angles below 90˚ and these particles are found to be presumably remains on the surface of substrate. Since decomposition of the hydrocarbons depends on catalytically activity of the particle surface that provides carbon atoms will only connect with already existing carbon structures present at the particle whisker interface. Thus, the oldest part of whisker is that the tip whereas the youngest part is at the bottom. This can be why, it's termed because the base growth mode. On the opposite hand, if there's a repulsive interaction between particle and surface then, a contact angle quite 90˚ are established. The particle then presumably detaches itself from the surface and lifts itself up. During this case, thus, the oldest part of CNT is nearest to the substrate surface whereas the youngest part is tip. Thus, this can be termed because the tip growth mode.

In the **figure 3.2** it's showed that the metal particles on the surface are exposed to vaporized hydrocarbons that decompose catalytically on the surface of the catalyst particle. An

exothermic decomposition is assumed and a carbon concentration also as a gradient type. On its decomposition the carbon diffuses from the recent space with a better concentration to the colder region of the particle and precipitates to create the graphitic structure of the CNT wall. The particle remains hooked up to the substrate.

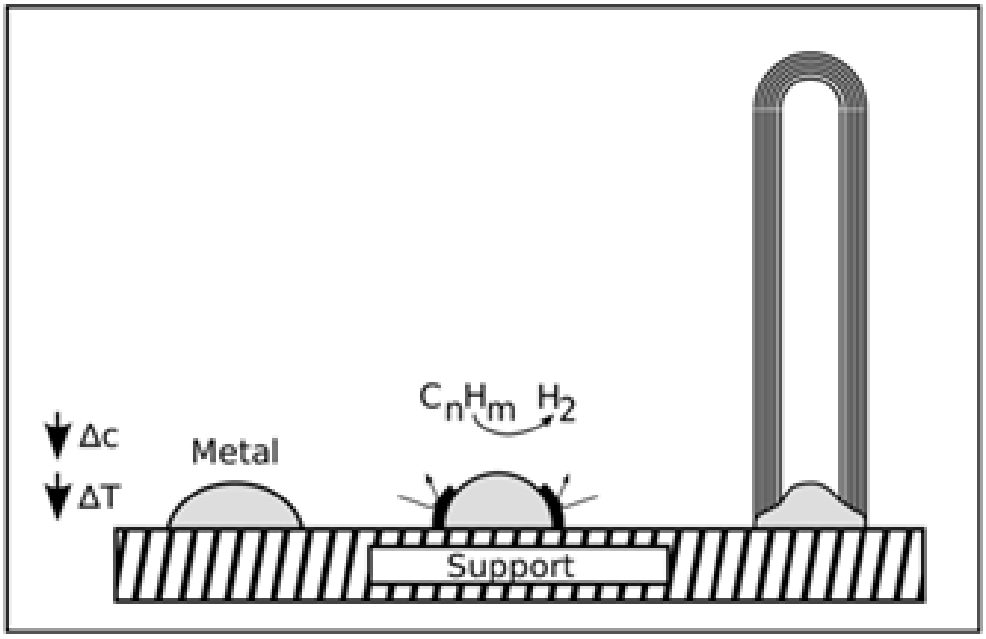

Fig 3.2 Base Growth Modes **[59]**

In the figure 3.3 it's showed that the metal particle is just infirm certain to the substrate surface. The decomposition of the hydrocarbons takes place at the top of the particle. Again associate degree exoreic decomposition is assumed and also the temperature and carbon concentration will increase at the highest of the particle that gets distorted throughout this method and detaches from the substrate. The carbon currently diffuses to the colder aspect of the particle and precipitates to create the CNT shells.

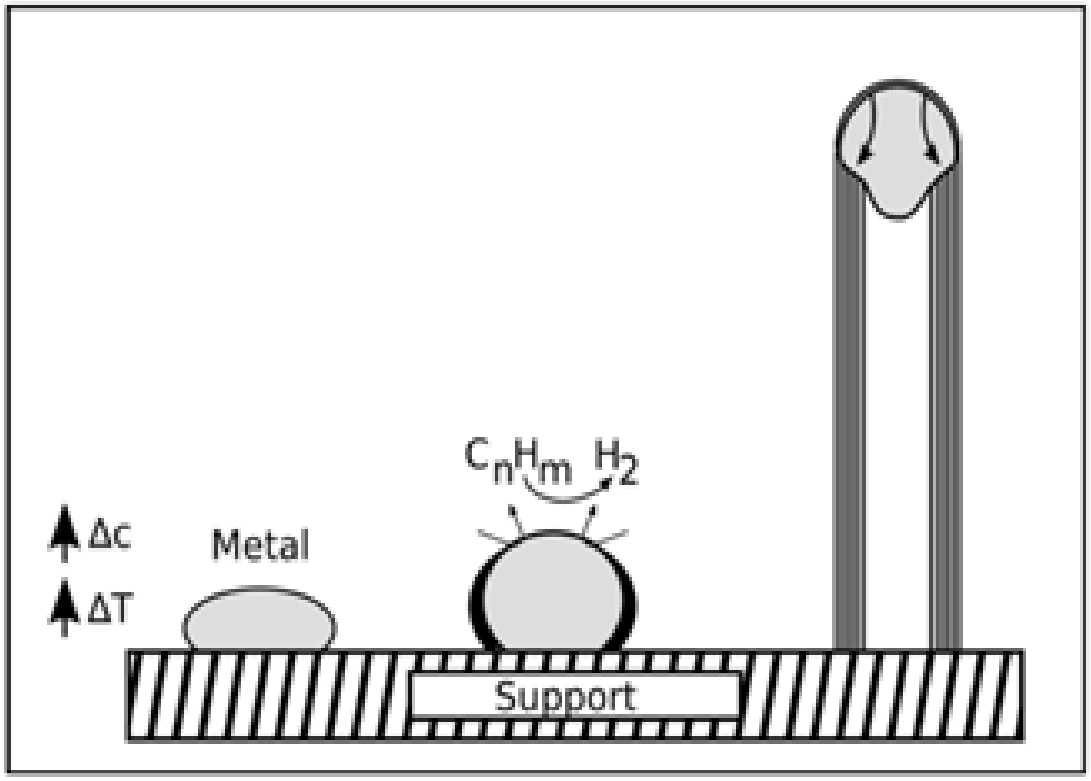

Fig 3.3 Tip Growth Mode **[60]**

3.1.2. Ligand assisted solid liquid growth mechanism (LSS)

Nanostructured CuO has been grown on Cu substrate after the reaction time of 96 h. Final samples show shiny black surface uniformly distributed all over the surface of Cu substrate indicating the formation of CuO which was further confirmed by SEM, TEM and XRD measurements. The nanostructured CuO are fabricated by a simple coordination self-assembly method in an alkaline solution with Cu^{2+} ions being from the surface oxidation of copper. In the present work, nanostructured CuO were synthesized by the decomposition of $[Cu(NH_3)_4]^{2+}$ precursor directly under the condition of reaction of time. The Cu substrate was oxidized by solution of NaOH and NH_3 which obeys following chemical reaction **[53].**

$$Cu + O_2 + H_2O + NH_3 \rightarrow [Cu(NH_3)_4]^{2+} \quad (1)$$

$$[Cu(NH_3)_4]^{2+} + 2OH^- \rightarrow Cu(OH)_2 \quad (2)$$

$$Cu(OH)_2 \rightarrow CuO + H_2O \quad (3)$$

The alkaline nature of Ammonia provides a basic media and adjusts the pH value of solutions. Also It co-ordinate with Cu^{2+}, giving rise to $Cu(NH_3)_4]^{2+}$complex which act as a molecular transporter that transports Cu^{2+} to the growing crystals with OH^- ions attached leading to the formation of $Cu(OH)_2$. The $Cu(OH)_2$ is unstable in alkaline solution and reduced to CuO **[54]**.

Nanorods growth mechanism can be interpreted via vapor-liquid-solid (VLS) and vapor-solid-solid (VSS) growth mechanism which is done only in presence of metal catalytic particles. In absence of these particles their growth mechanism can be implemented by ligands aided solution-solid (LSS) growth mechanism **[55]**. Here we report the mechanism of nanorods and nanowires via LSS because solution contains no catalyst. According to this growth mechanism coordination self assembly of $Cu(OH)_2$ occurs at solid liquid interface in an aqueous solution **[56]**. $Cu(OH)_2$ is a layered material and its orthorhombic crystal structure helps in assembly of nanorods and nanowires. Cu^{2+} prefers coordination with OH^- **fig 3.4 (A)** and this leads to formation of extended chain, which can be connected through the OH^- legands **fig 3.4 (B)**. Cu foil with large and open surface area is used as controlled delivery source of Cu^{2+} in aqueous solution under oxidative and alkaline conditions. This means that $Cu(OH)_2$ nucleates and grows in one dimension by itself with the aid of ligands **fig 3.4 (C).** But in alkaline solution $Cu(OH)_2$ gets reduced to CuO and forms nanorods and nanoflowers **[57].**

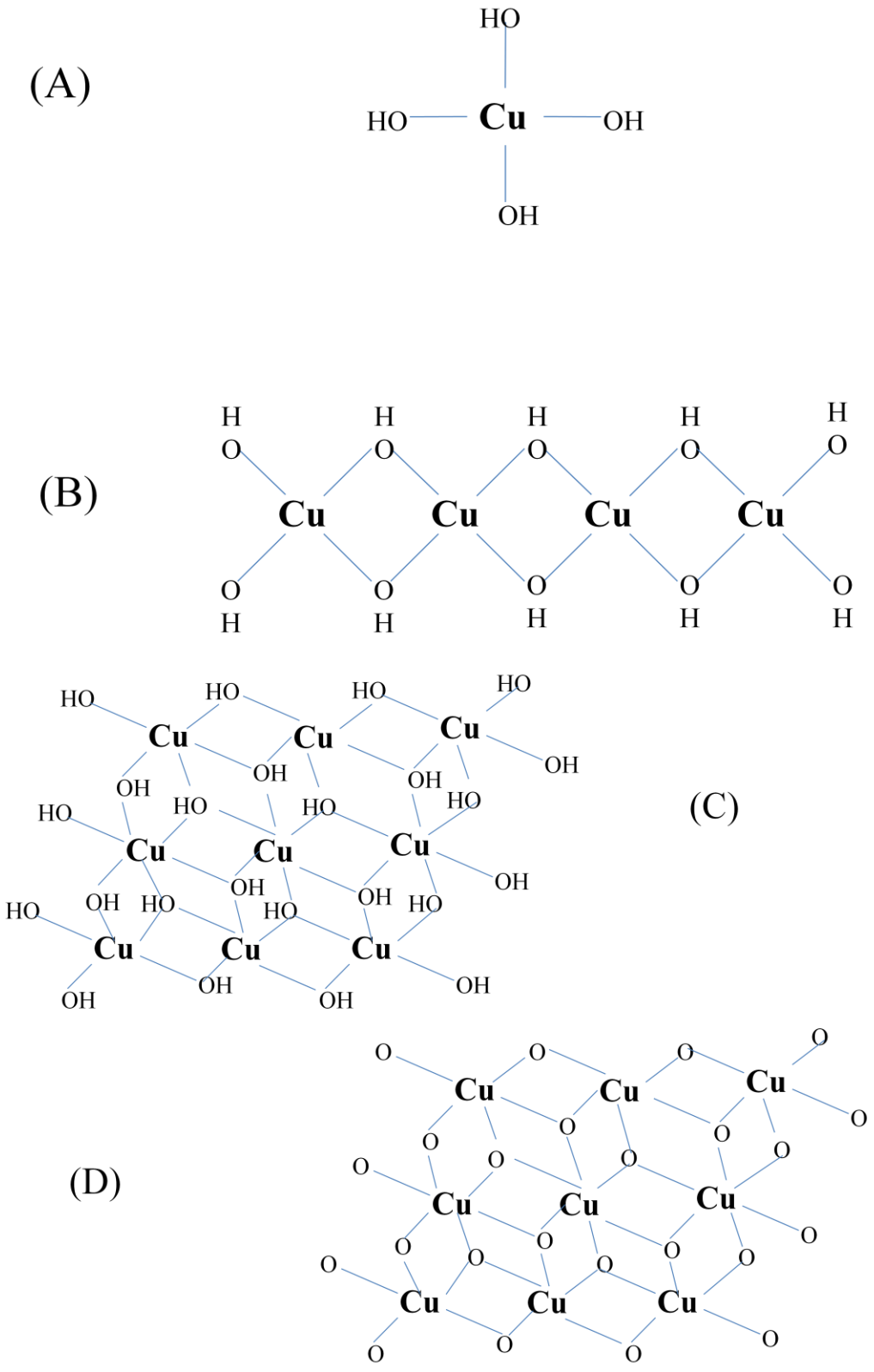

Fig 3.4 Schematic Showing the Coordination Assembly Growth of CuO Nanostructures

The formation of CuO nanorods and nanoflowers can be discussed by the growth mechanism described in **fig 3.5.**

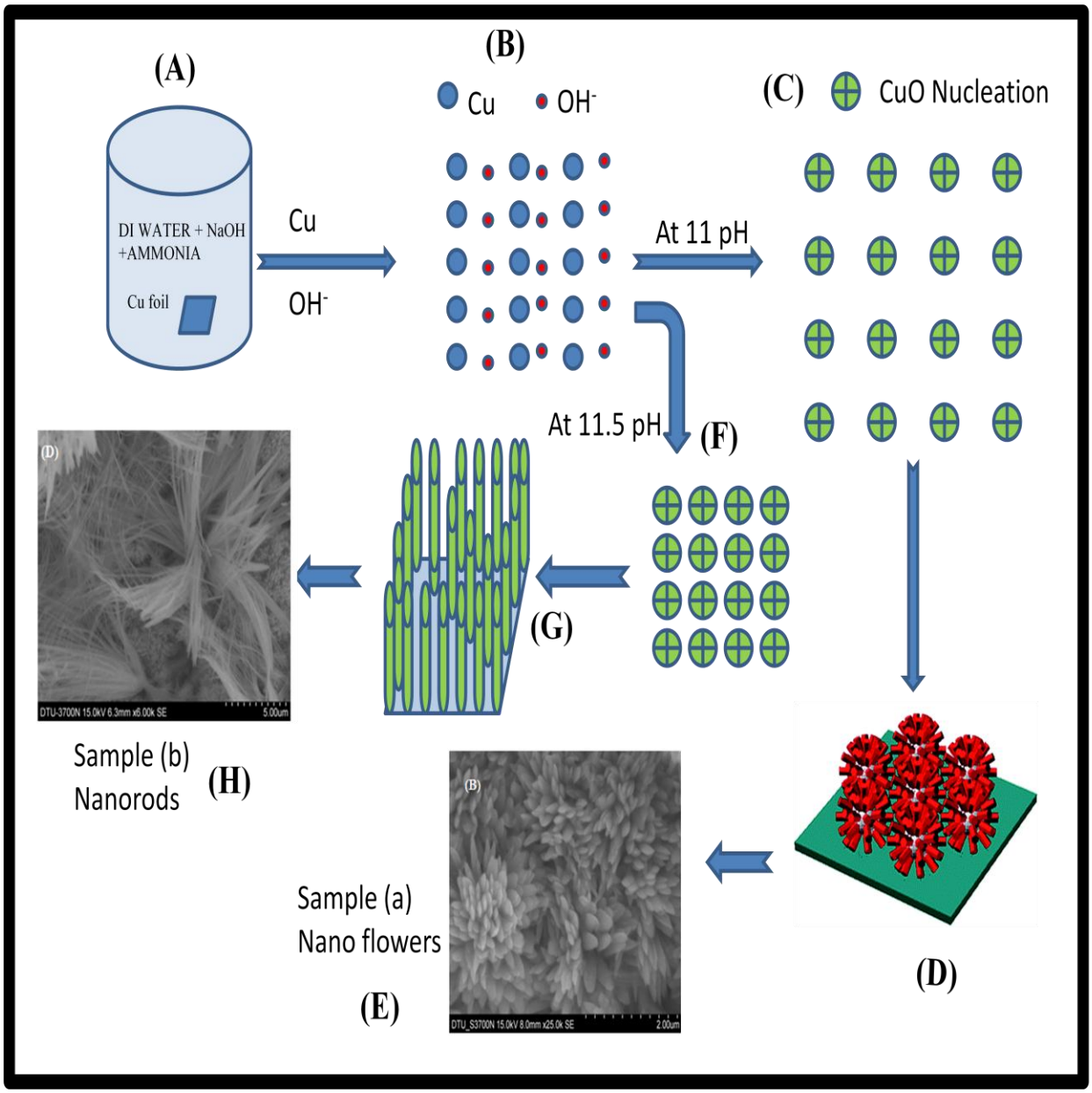

Fig 3.5 Scheme representing the possible growth mechanism of the formation of CuO nanostructures

As discussed earlier according to these chemical reactions, NH_3 reacts with DI water H_2O and produces ammonium ions and OH^- ions **(A).** This stage controls the concentration of OH^- ions which is most important for formation of CuO nanostructures. Concentration of OH^- ions varies according to pH value of solution. As pH of solution increases from 11 to 11.5 and 12, concentration of OH^- ions also increases. Firstly initiation starts in which reaction slowly generates building units of $Cu(OH)_2$ at Cu substrate until a crucial super-saturation level is reached and nucleation starts **(B)**. The $Cu(OH)_2$ nanostructures are fabricated by a simple coordination self-assembly method in an alkaline solution with Cu^{2+} ions being from the surface oxidation of copper. In sample (a) (at 11 pH), the concentration of OH^- ions is comparatively low which causes rare concentration of nucleation sites **(C).** Further CuO nanorod grows according to bottom up approach but due to distance and large gap between nucleation sites nanorods can be grew towards various directions **(D)**. Thus CuO shapes into nanoflowers. In sample (b), pH of solution increases up to 11.5 which increase concentration of nucleation sites **(F)**. Densely packed crystalline nucleation site allows CuO to grow only in one direction which results into aligned nanorods **(G)**. In sample (c), pH of solution increases to 12 which cause denser nucleation sites than sample (b). Highly concentrated nucleation sites allow formation of densely packed nanorods.

Chapter 4

Experimental procedures

In this chapter we will discuss all the experimental procedures carried out throughout span of project, their setups and precursor material used. Here wet chemical method is used to fabricate nanorods, nanoflowers and nanowires. All the experimental was carried out in nuclear lab, applied physics department, DTU.

4.1 Synthesis technique adopted: Wet chemical method

Wet chemical route is simplest of all synthesis methods of CuO nanostructures because in this process there is no need of high pressure and high temperatures. It can be processed under ambient temperature and pressures. This method also needs no costly equipments for fabrication such as CVD setups, Arc discharge setups, laser ablation setups. All these above mentioned methods are very costly and highly précised. But this method which is adopted is simple and cost effective and can be performed easily.

4.2 Experimental procedures for CuO nanorods, nanoflowers, and dense nanorods

4.2.1 Required apparatus and chemicals

In order to complete the entire set up of experiment a number of apparatus and precursors are needed, here in this topic we will name and if necessary, explain each one of them.

1. Beakers: Three beakers of capacity 500 ml are taken in which sample will be drowned for required time.
2. De Ionized water : 400 ml of DI water is needed for experiment
3. Sodium Hydroxide: NaOH of 1M solution is required.
4. Ammonium solution: NH_3 solution is used in this method. 13 M NH_3 solutions have been made.
5. Cu Foil: purity 99.9% Cu of dimension 1×1 cm^2 with thickness 0.15 mm is used in this process. CuO nanostructures have been grown on this foil by oxidation of Cu on their surface.

4.2.2 Experimental

At First, three copper foils (purity: 99.9% Cu) of dimension 1×1 cm^2 with thickness 0.15mm were burnished by abrasive paper followed by thorough cleaning by DI water and absolute ethanol to remove absorbed dust and surface contamination. These foils were immersed in 4M HCl solution for 15 min so that residual oxide layer could be removed. 1M NaOH solution was prepared by adding 0.8 gm of NaOH in 20ml of DI water and 13M NH_3 solution was prepared by adding 2.842 ml of NH_3 in 10ml of DI water. These foils were immersed in the following three solutions having different pH value after washing them three times with deionized water Sample (a) was dipped in solution containing 400 ml of DI water, 1 ml of ammonia and 2 ml of NaOH for 96 h at pH 11. Sample (b) was dipped in solution containing 400ml of DI water, 2 ml of ammonia and 3 ml of NaOH for 96 h, at pH 11.5. Sample (c) was dipped in solution containing 400ml of DI water, 1ml of ammonia and 10 ml of NaOH for 96 h, at pH 12. The samples (a, b and c) were taken out of respective solutions and washed with deionized water. Uniformly deposited black films were observed on the surface of the samples. As prepared samples were analyzed using scanning electron microscopy (SEM) and X-ray powder diffraction (XRD).

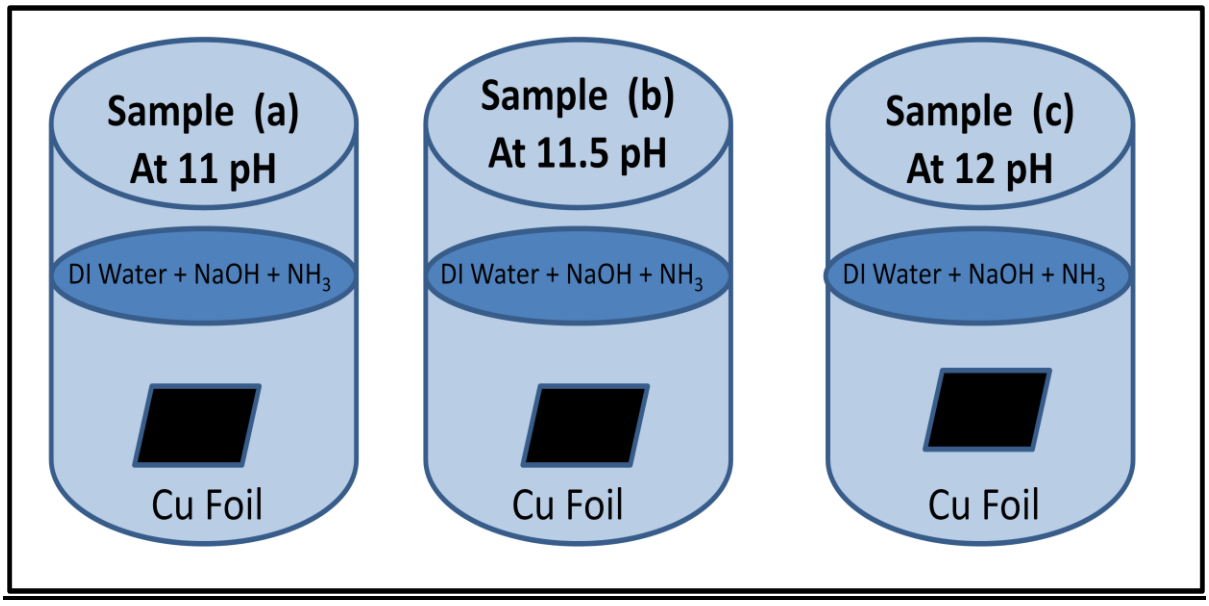

Fig 4.1 Scheme for synthesis of CuO nanorods

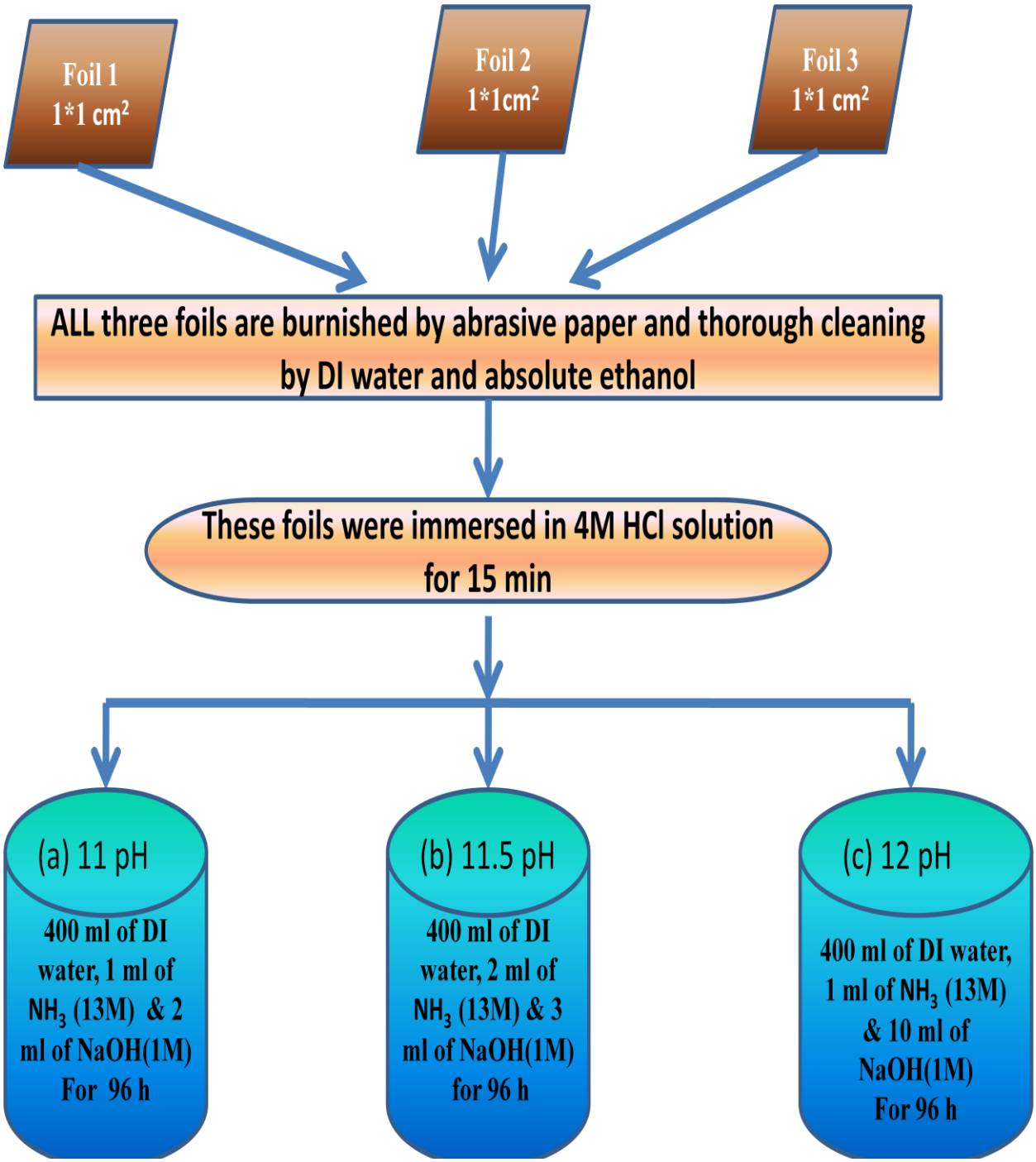

Fig 4.2 Illustration of Experimental process for synthesis of CuO nanorod and nanoflowers

4.3 Experimental procedures for CuO nanowires

4.3.1 Required apparatus and chemicals

In order to complete the entire set up of experiment a number of apparatus and precursors are needed, here in this topic we will name and if necessary, explain each one of them.

1. Beakers: One beaker of capacity 100 ml is taken in which sample will be drowned for required time.
2. Copper acetate [$(CH_3COO)_2$-H_2O] as precursor has been taken to prepare a solution of 0.5 M solution of Copper acetate in DI water.
3. Sodium Hydroxide: NaOH of 5M solution is required.
4. Poly Ethylene Glycol (PEG) 1 ml is required.
5. De Ionized water : 40 ml of DI water is needed for experiment

4.3.2 Experimental

Firstly, Copper acetate [$(CH_3COO)_2$-H_2O] has been taken as precursor and required amount of it has been mixed with 20 ml of De ionized water. This solution has been stirred for 10 min and denoted as solution A. On other hand required amount Sodium Hydroxide (NaOH) has been taken to make a 5M solution in 20ml of De ionized water. This solution also has been stirred for 10 min. This solution has been denoted as Solution B. After ample of stirring, both solution has been mixed and stirred thoroughly. 1ml of Poly Ethylene Glycol (PEG) is mixed drop wise which act as directional reagent. Water is mixed instantly and continued stirring for few more minutes. After that precipitates has been collected by centrifugation which has been dried over night. Powder form sample has been taken for further characterization. This sample has been denoted as Sample (D).

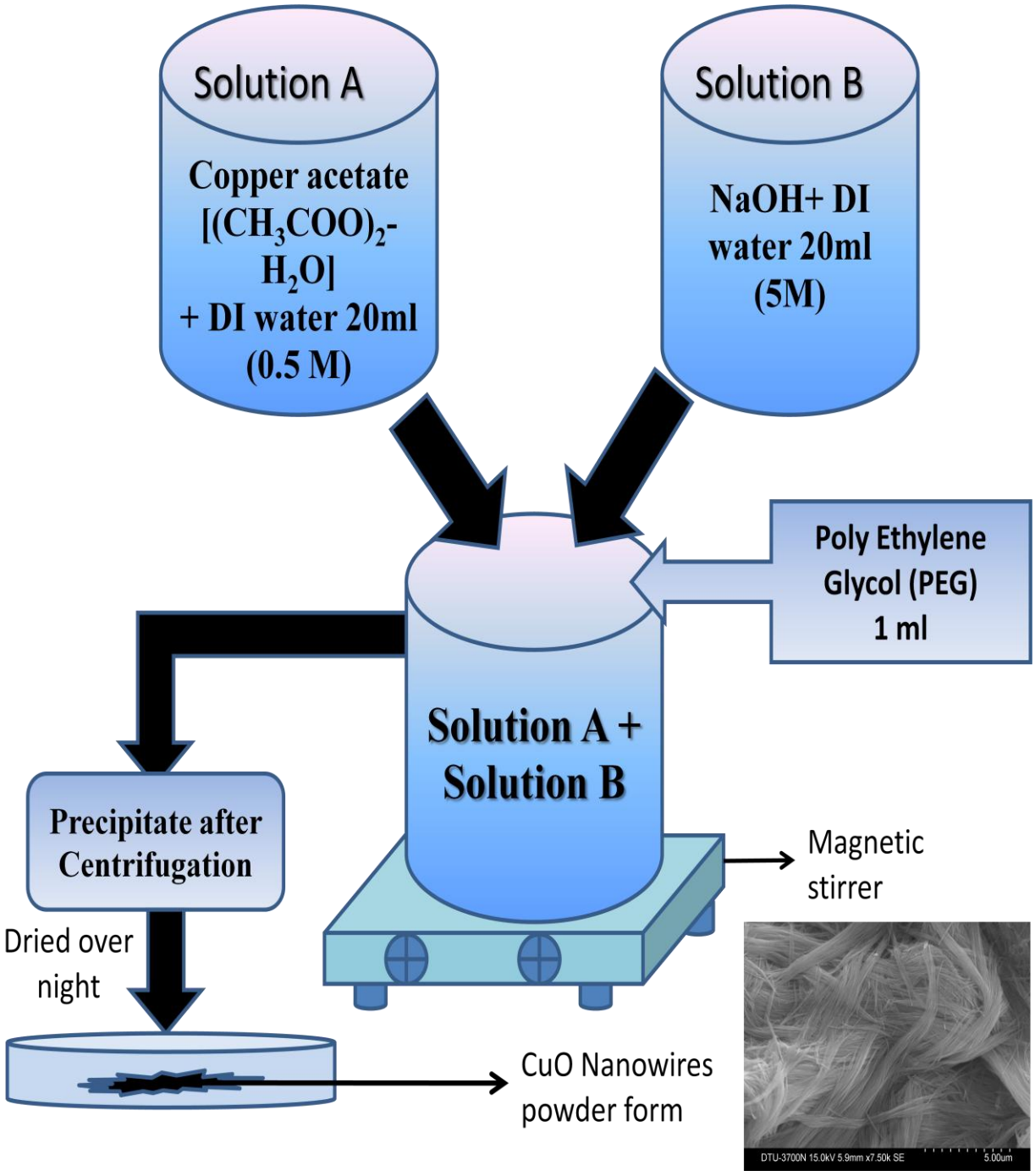

Fig 4.3 Illustration of Experimental process for synthesis of CuO nanowires

Chapter 5

5.1 Methods of Characterization

Characterization techniques are referred to those methods through which one can identify an as-prepared sample with respect to its morphology, surface topology, internal structure, composition, etc. These techniques used to study the properties, features, tolerance of a sample to the imposed environment so that during the process, no damage is done to the sample either internally or externally.

In order to analyze the as-grown CuO nanostructures samples, a few characterization techniques are capable of characterizing them at a microscopic and below scale were necessary as the crystal compound growths were expected to be up to several nanometers in size. On account to get the information about surface morphology, direction of planes crystallite size of samples, information about metal oxide bonding and dimensions of nanostructures some powerful techniques are adopted. The set up and working of these techniques are briefly summarized below.

5.1.1 X-Ray Diffraction (XRD)

X-ray diffraction analysis technique has been used to get information about miller planes, crystallite size of samples. It uses the intensities and spatial distribution of X-rays radiation scattered by the sample samples because crystals have a rigid periodicity in structure and constitutes naturally produced diffraction gratings for X-rays. When these X-rays colloids with the particles of sample, X-ray are diffracted accordingly due to electron and x-ray collision. The wavelength and structure of sample particle affects the pattern of X-ray diffraction.

Crystals are basically regular arrays of atoms in which atoms are arranged in a periodic manner. When X-ray waves interact with the periodic atoms then scattering of waves occur in backward direction and X-ray striking the electron produces secondary spherical waves emerging from the electron. This phenomenon is called as elastic scattering, and the electron is called as the scatterer. A regular array of spherical waves is produced by these atoms of a sample. The constructive interferences of forward and backward waves are responsible to get the information

about XRD which can be determined by Bragg's law. Hence, X-ray diffraction results from an electromagnetic wave (the X-ray) impinging on a regular array of scatterers (the repeated arrangement of atoms within the crystal).

When X-rays having wavelength λ which is typically the same order of magnitude (1–100 angstroms) interact with planes in the sample's crystal spacing *d* between them, produce the diffraction pattern. According to the Bragg law, diffraction happens only if the stated condition is verified

$$2d\sin\theta = n\lambda$$

With particular diffraction angle (θ), incoming x-ray wavelength (λ) is related to the planar distance of crystals (d), as shown in the figure below. XRD is a non-destructive analytical method to identify phase as well as orientation, to determine structural properties, to measure the thickness of thin films, estimate the size of nanoparticles, etc.

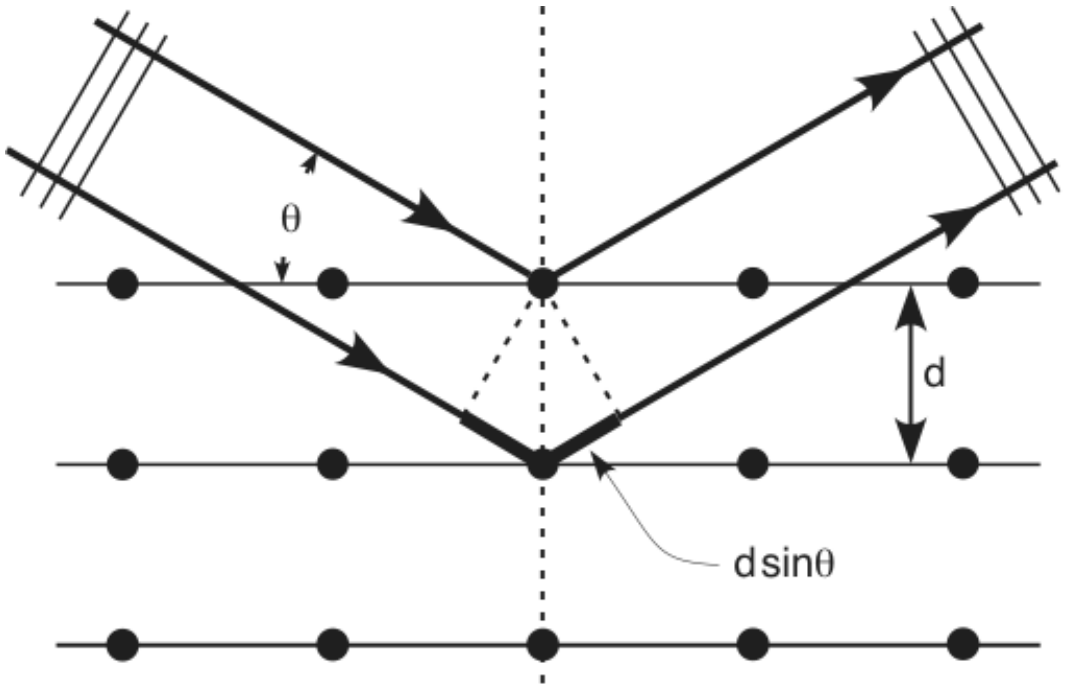

Fig 5.1 Bragg diffraction **[61]**

Fig 5.2 Picture of XRD set up @DTU

5.1.2 Scanning Electron Microscopy (SEM)

It is a type of electron microscope that creates images of a sample by scanning the sample with a focused beam of electrons. It produces many types of signals when electrons interact with the sample's atom that can be detected and deduce the information about the sample's surface topography and composition. The electron beam is usually scanned in a raster scan pattern and to produce an image the position of the beam is combined with the detected signal. The electron beams excite the secondary electrons from the sample surface which are mostly detected by SEM. The amount of secondary electrons depends on the angle at which beam meets specimen surface, i.e. on specimen topography. In a Scanning electron microscope, there is a special kind of detector that can be used to detect and collect the secondary electrons by scanning the sample.

Thus an image displaying the topographical information of the surface is formed, revealing Shape and size of sample having minute details less than 1 nm in size.

SEM is typically consisted of the following features:

- A source (electron gun) of the electron beam which is accelerated down the column.
- A series of lenses (objective and condenser) which act to control the diameter of the beam as well as to focus the beam on the specimen.
- An area of beam/interaction which generates several types of signals that can be detected and processed so as to produce an image or spectra.
- A series of apertures (micro scale holes in metal films) through which the beam passes and which affects properties of that beam.
- Controls for specimen position (x, y, z-height) as well as orientation (tilt, rotation).
- All the above components are maintained at high vacuum levels.

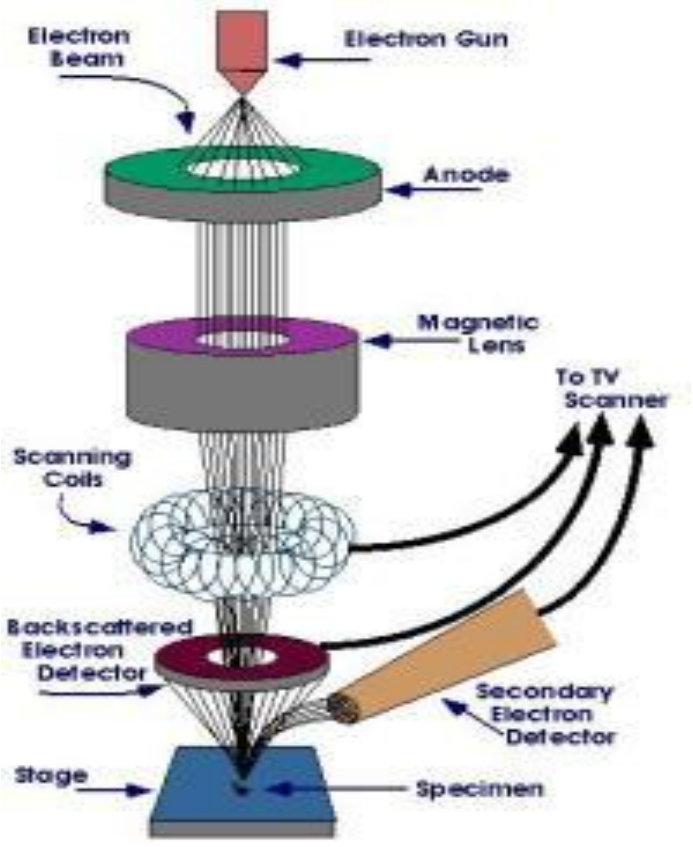

Fig 5.3 Schematic of SEM apparatus **[62]**

Fig 5.4 Picture of SEM set up @ DTU

A thermionic electron beam of SEM is emitted from an electron gun that is equipped with a tungsten filament cathode. The electron beam has an energy generally ranging from 0.2 to 40 KeV, this beam is pointed by one or two condenser lenses to a spot that is about 0.4 nm to 5 nm in diameter. The beam then passes through pairs of deflector plate or couple of scanning coils present in electron column, and finally through deflector lens, which deflect the beam and scan in a raster fashion to cover a rectangular area in the x and y axes of the sample's surface. This

process starts from left to right and from top to bottom. There is a direct one-to-one correspondence between the pattern of the specimen and the rastering pattern that is being used to produce the image on monitor. The number of pixels in each row as well as the total number of rows of the scanned area is affected by the resolution chosen to image. When primary beam of electrons passing through focusing lenses interacts with the sample, the electrons loses their energy by repeated random absorption and scattering within the interaction volume, which is normally less than 100 nm to approximately 5 μm into the surface. The types of signals produced by a SEM include back-scattered electrons (BSE), secondary electrons (SE), characteristic X-rays, Auger electrons and light (cathodoluminescence) (CL).

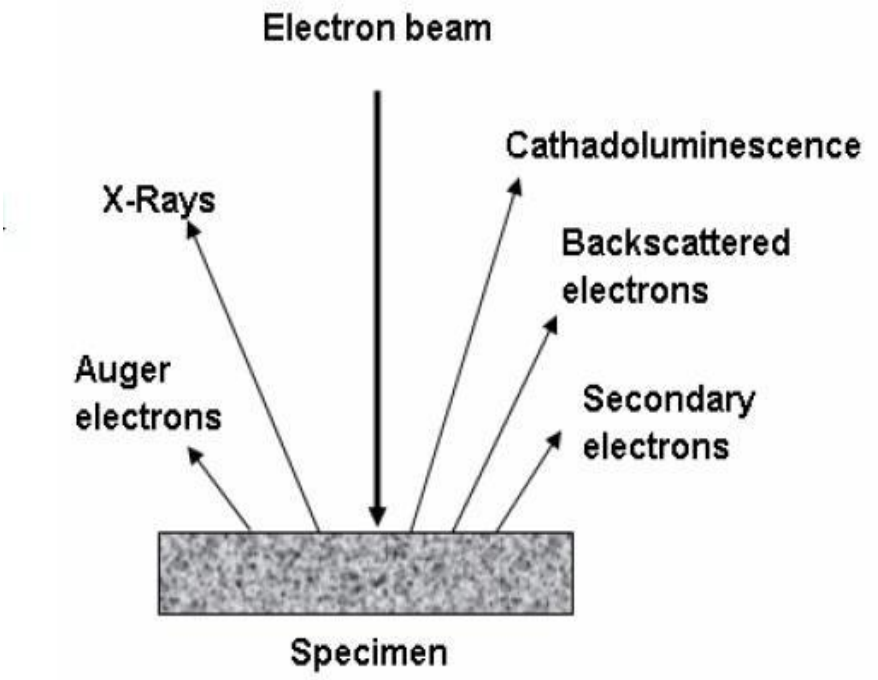

Fig 5.5 Different types of electrons released during SEM imaging **[63]**

a) **Secondary Electrons**: If an incident electron collides with an electron in a sample atom, electron will be knocked out of its orbital shell and the atom becomes ionized. Multiple collisions are possible because the incident electron loses only a little energy during each collision; hence, continuing until the occurrence electron has no more energy to extricate secondary electrons. Each freed secondary electron has a small kinetic energy (<50 eV),

which is independent of the energy of the incident electron. These secondary electrons can escape from the sample and can be collected by the detector. As a result, sample topography can be seen through secondary electron imaging.

b) **Backscattered Electrons**: If an electron interacts with the nucleus of a surface atom, then the electron will bounce back or scatter 'backward' out of the sample as a backscattered electron (BSE). These backscattered electrons have high energies, typically in the range of 50 eV. Atomic number of sample affects the no of BSE electrons thus the production of these BSE electrons varies directly with atomic no and to distinguish differences in sample atomic number, backscattered electron images can be used.

c) **Auger Electrons:** A vacancy is left in an ionized atom's electron shell due to generation of secondary electron. In order to fill this vacancy, an electron from a higher energy outer shell (from the same atom) can drop down to fill the vacancy. Due to this surplus energy in the atom an outer electron is emitted which is an Auger electron. Auger electrons have a characteristic energy unique to the element from which they are emitted. However, Auger electrons are only emitted from shallow sample depths (<3 nm) because they have a relatively low kinetic energy. These electrons can be used to give compositional information about the target sample.

d) **Characteristic X-rays**: When the incident electron beam colloids with the sample's surface, X-rays are also produced. These X-rays' excess energy is produced as a result of reshuffling electrons to fill shell vacancies just like the Auger electron generating process. X-rays provide compositional information about the sample because they have a characteristic energy unique to the element from which they are emitted.

5.1.3 Transmission Electron Microscopy (TEM)

In this microscopy technique the beam of electrons is made to transmit through a very thin specimen and interacts with it. An image is then formed by the interaction of the electrons which transmitted through the specimen, then the image is magnified and focused onto an imaging device, like a fluorescent screen, or on a layer of photographic film, or it can be detected by the use of a sensor. Due to the small de Broglie wavelength of the electrons, TEMs are capable of imaging at a much higher resolution than optical microscopes. Due to absorption of electrons in the material or due to the thickness and composition of the material TEM image contrast occur at

smaller magnifications. At much higher magnifications complex wave interactions modulate the intensity of the produced image, requiring professional analysis of observed images. Alternate modes of TEM are used to observe modulations in electronic structure, chemical identity, crystal orientation, sample induced electron phase shift and the regular absorption based imaging. TEM forms an important analysis methodology in a range of scientific fields, in both physical as well as biological sciences.

Very high energy electrons are used to penetrate through an ultrathin (≤100 nm) sample by Transmission electron microscopy (TEM). This can increase spatial resolution in imaging (down to individual atoms) and the possibility of carrying out diffraction from nano-sized volumes. When high energy electrons are accelerated up to few hundreds keV and focused onto a material, those electrons can scatter or might backscatter elastically or inelastically and produce many different signals such as X-rays, Auger electrons or light. Some of them can be used in transmission electron microscopy (TEM).

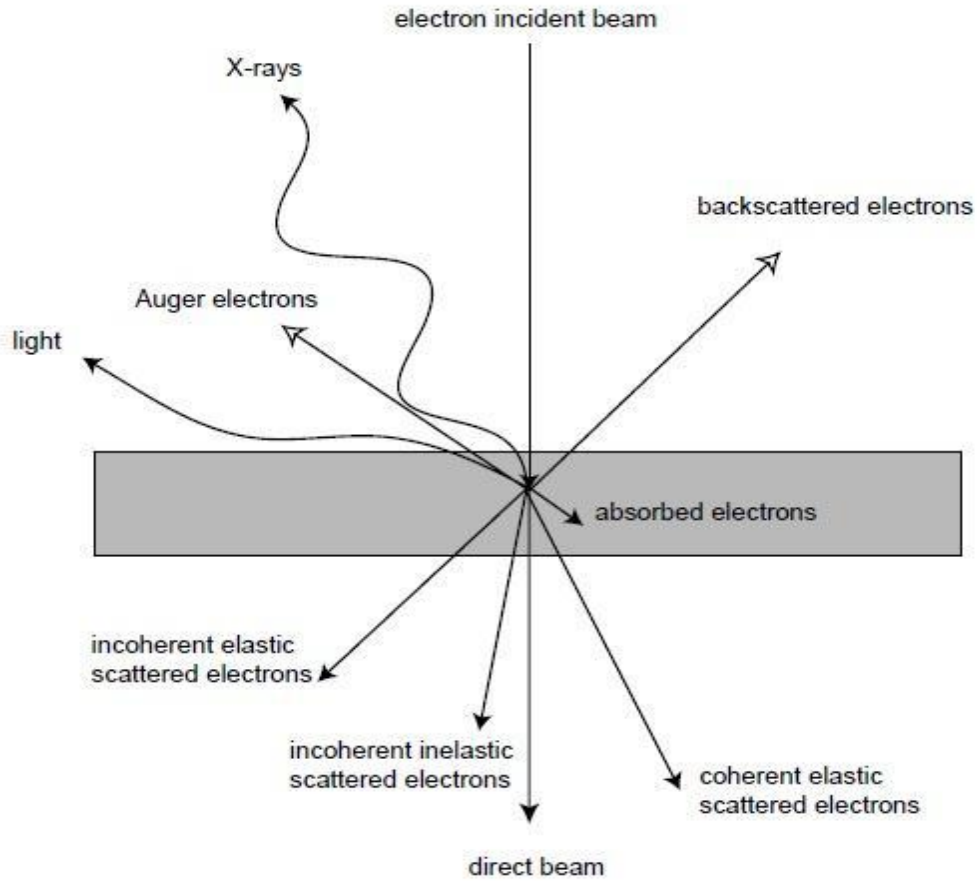

Fig 5.6 Different types of signals produced during TEM imaging **[64]**

Electrons exist in both wave and particle state thus they have both wave as well as particle properties (as theorized by Louis-Victor de Broglie). Electrons behave as an electromagnetic radiation due to their wave like property. The wavelength of electrons is affected by their kinetic energy via the de Broglie equation. In a TEM an electron's velocity reaches very close to the speed of light, *c*.

$$\lambda e \approx \frac{h}{\sqrt{2m_0 E\,(1 + \frac{E}{2m_0 c^2})}}$$

Where, h is Planck's constant, E is that the energy of the accelerated electron associated m0 is that the rest mass of an electron. Electrons are usually generated in an electron microscope by a specific notable method thermal emission generates electrons from a filament, usually tungsten, within the same manner as that of a light bulb, or by field electron emission. The electrons are then accelerated using an electrical voltage and targeted by electrostatic moreover as by electromagnetic lenses to the sample. The transmitted beam consist data concerning phase, electron density and periodicity; this beam is employed to make the image.

TEM operates principally in 2 modes, namely,

(A) Imaging Mode

(B) Diffraction Mode

A transmission electron microscope is formed up of:

(1) 2 or 3 condenser lenses to focus the electron beam onto the sample,

(2) An objective lens so as to make the diffraction within the back focal plane and therefore the image of the sample on the image plane,

(3) Some intermediate lenses to amplify the image or the diffraction pattern on the screen.

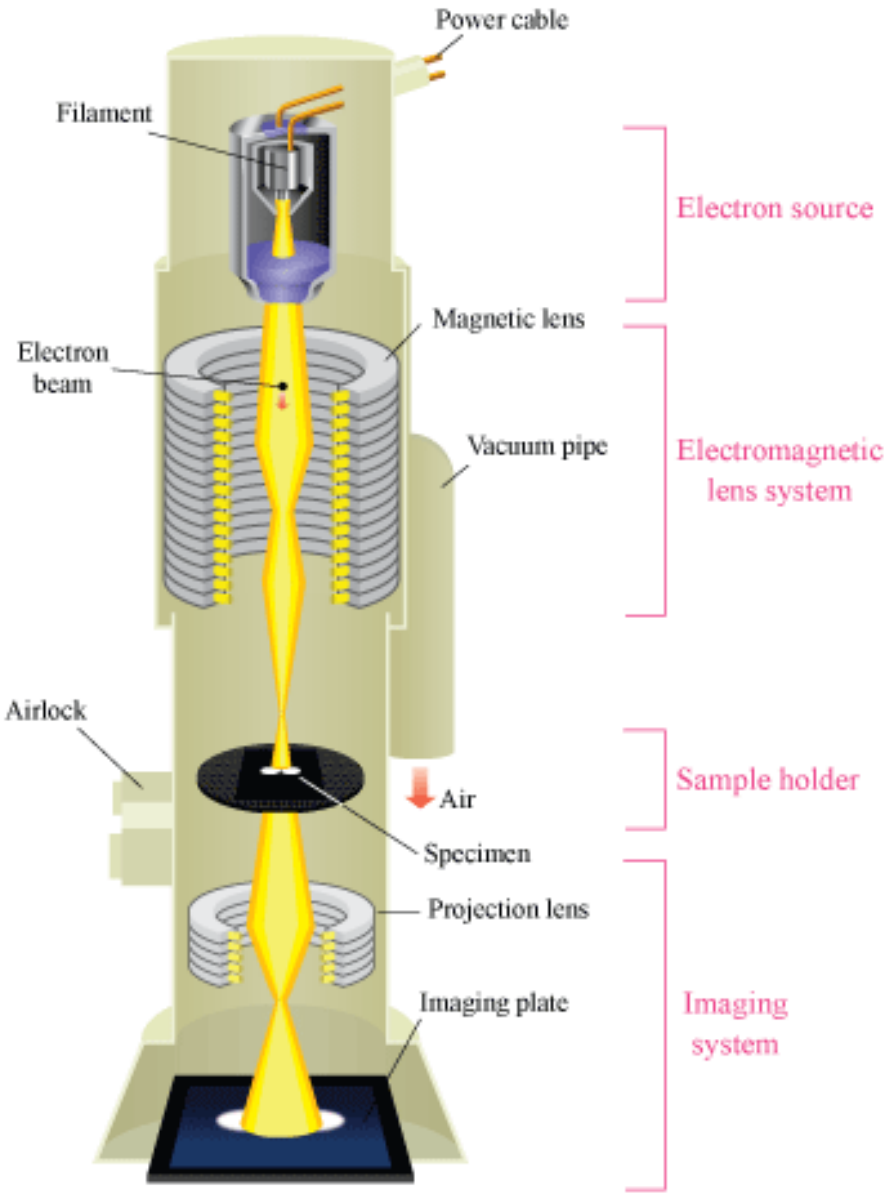

Fig 5.7 Schematic Diagram of TEM **[65]**

Fig 5.8 image of TEM established @JNU

(A) Imaging mode

If the sample is thin (< 200 nm) and formed of early periodic table chemical components, the image presents a really low contrast when it's targeted. To induce amplitude contrasted image, an objective diaphragm has to be inserted within the back focal plane to pick the transmitted beam. The crystalline elements in Bragg orientation seems to be dark and not Bragg directed elements or the amorphous seem bright. This kind of imaging mode is named bright field mode BF. If the diffraction is created of several diffracting phases, every of them will separately be differentiated by choosing one in all its diffracted beams with the assistance of objective diaphragm. To do so, the incident beam should be angled so the diffracted beam is placed on the target lens axis to

avoid off axis aberrations. This mode is thought as dark field mode DF. The intense field and dark field modes are used for imaging materials to nanometer scale.

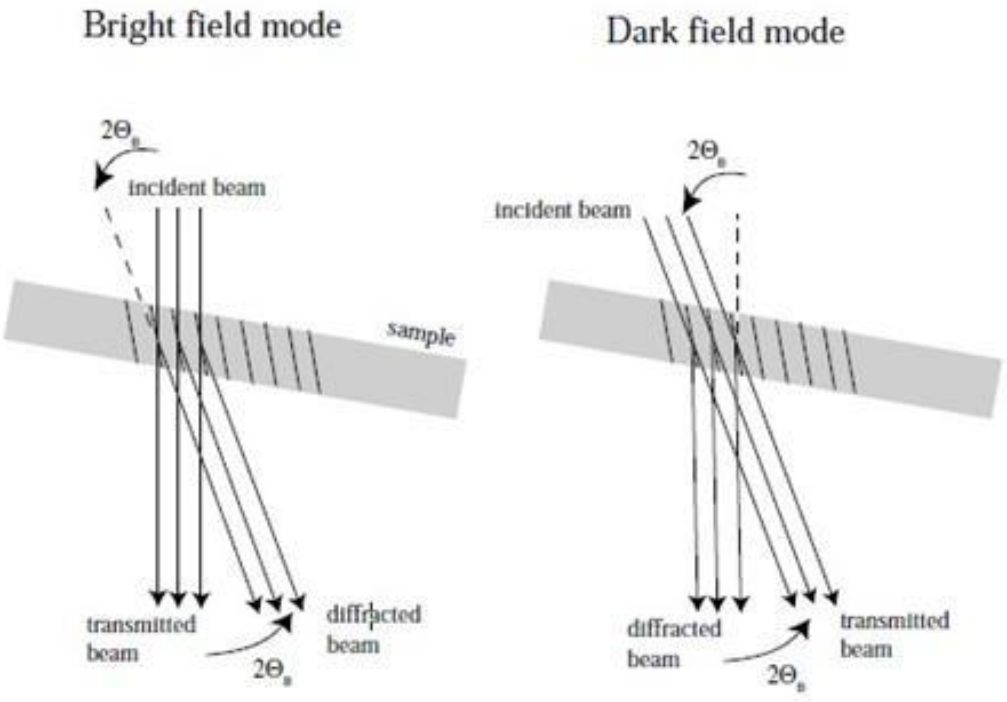

Fig 5.9 Bright and dark field modes for imaging **[66]**

(B) Diffraction Modes

The selected area diaphragm is employed solely to pick out one a part of imaged sample for example a particle or a precipitate. This mode is thought as chosen area diffraction SAED. The spherical aberrations of the target lens prohibit the area of the chosen object to few hundreds of nanometers. However, it's potential to get diffraction patterns of tiny object by focusing the electromagnetic radiation with the projector lenses to get a small spot size on the article surface (2-10 nm). The spots of SAED become disks whose radii rely upon the condenser diaphragm. This can be referred to as micro diffraction.

SAED and micro diffraction patterns of a crystal allow getting the symmetry of its lattice and these calculate its interplanar distances (with the Bragg law). This can be helpful to substantiate the identification of a section, once assumptions typically supported the literature of the studied system and on chemical analyses.

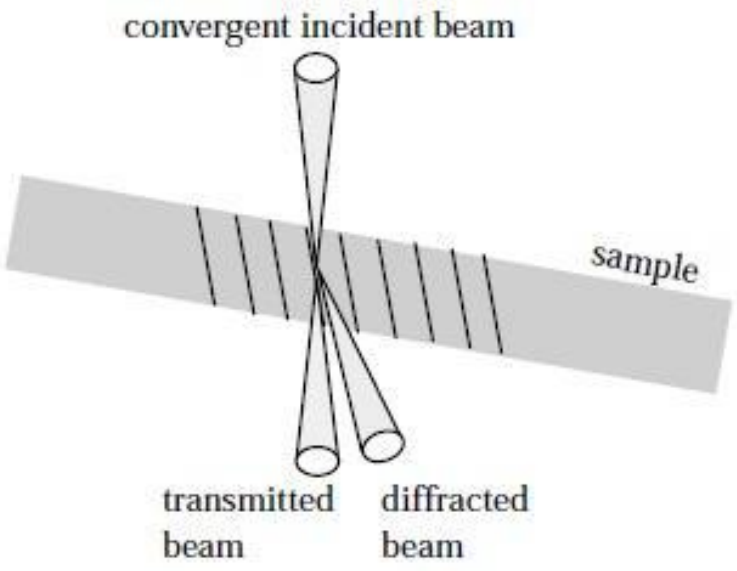

Fig 5.10 Diffraction Mode **[67]**

5.1.4 FTIR spectroscopic analysis

FTIR (Fourier transform Infrared) or just FTIR Analysis, is most helpful technique for distinguishing chemicals that are either organic or inorganic. It is used to quantities some parts of an unknown mixture. It is applied to the analysis of liquids, gasses and solids. FTIR spectroscopic analysis could be a multiplexing technique, wherever all optical frequencies from the supply are discovered at the same time over a amount of time referred to as scan time. During this technique whole information is collected and regenerated from an interference pattern to a spectrum.

By interpreting the infrared absorption spectrum, the chemical bonds (functional groups) during a molecule or molecular structure of materials, whether or not organic or inorganic is determined. FTIR spectra of pure compounds are typically so distinctive that they're sort of a molecular "fingerprint". Whereas organic compounds have terribly rich, elaborated spectra, inorganic compounds are typically easier. The technique works on the very fact that bonds and groups of bonds vibrate at characteristic frequencies. A molecule that's exposed to infrared rays

absorbs infrared energy at frequencies that are characteristic to that molecule i.e. those frequencies where the infrared radiation affects the dipolar moment of the molecule. So monoatomic (He, Ne, Ar, etc) and homopolar diatomic (H_2, N_2, O_2, etc) molecules don't absorb infrared radiation throughout FTIR analysis, a spot on the specimen is subjected to a modulated IR beam. The specimen's transmission and coefficient of reflection of the infrared rays at totally different frequencies is translated into an IR absorption plot consisting of reverse peaks. The ensuing FTIR spectral pattern is then analyzed and matched with notable signatures of known materials within the FTIR library. IR absorption data is usually bestowed within the kind of a spectrum with wavelength or wave number as the coordinate axis and absorption intensity or % transmission as the coordinate axis transmission, T, is that the quantitative relation of radiant power transmitted by the sample (I) to the radiant on the sample (I_0). Absorbance (A) is that the logarithm to the base 10 of the reciprocal of the transmittance (T).

$$A = \log_{10} \frac{1}{T} = -\log_{10} T = -\log_{10} \frac{1}{I_0}$$

The transmission spectra give higher distinction between intensities of strong and weak bands as a result of transmission ranges from zero to 100% T whereas absorbance ranges from infinity to zero.

The recording Cartesian coordinate range of this instrument is 400-4000cm–1. Every spectrum was collected with 64 scans co-added at 4cm–1 resolution. The traditional operation mode of this spectrometer is temperature stabilized. The spectrometer utilizes continuous dynamic alignment to make sure exceptional high-resolution line shapes. Its compact optical path minimizes beam path length and improves spectral performance by limiting the quantity of beam reflections that interprets into extraordinarily reproducible results with no instrument drift. Before measure the instrument is correctly sealed and desiccated. The desiccant protects the beam splitter and alternative optical parts by reducing the quantity of water vapor within the spectrometer.

Chapter 6

6.1 Results and Discussions

6.1.1 Scanning Electron Microscope

Fig 6.2 shows SEM images of nanostructured CuO having various length and density deposited on copper substrate at different pH value and reaction time. It is evident from the images that nanorods cover the surface of substrate uniform and compactly. **Fig 6.2 (a)** shows flower like structure of sample (a) which is processed at pH 11. **Fig 6.2(b)** shows higher resolution image of flower pellets in sample (a). Whereas sample (b) has nanorods like structure of length 100-200 nm, as visible in **fig 6.2(c)** and **6.2(d)**. Sample (c) represents dense nanorods compared to sample (b). **Fig 6.2(e)** and **6.2(f)** show SEM images of sample (c). Thus, it can be seen from SEM images that on increasing pH of solution, the density of nanostructured CuO increases and results in nanoflowers and nanorods.

Whereas CuO nanowires synthesized by wet chemical method having other precursor materials shown in **fig 6.1.** In this SEM image nanowires are clearly shown which are 10-15 nm in diameter and several nm in length.

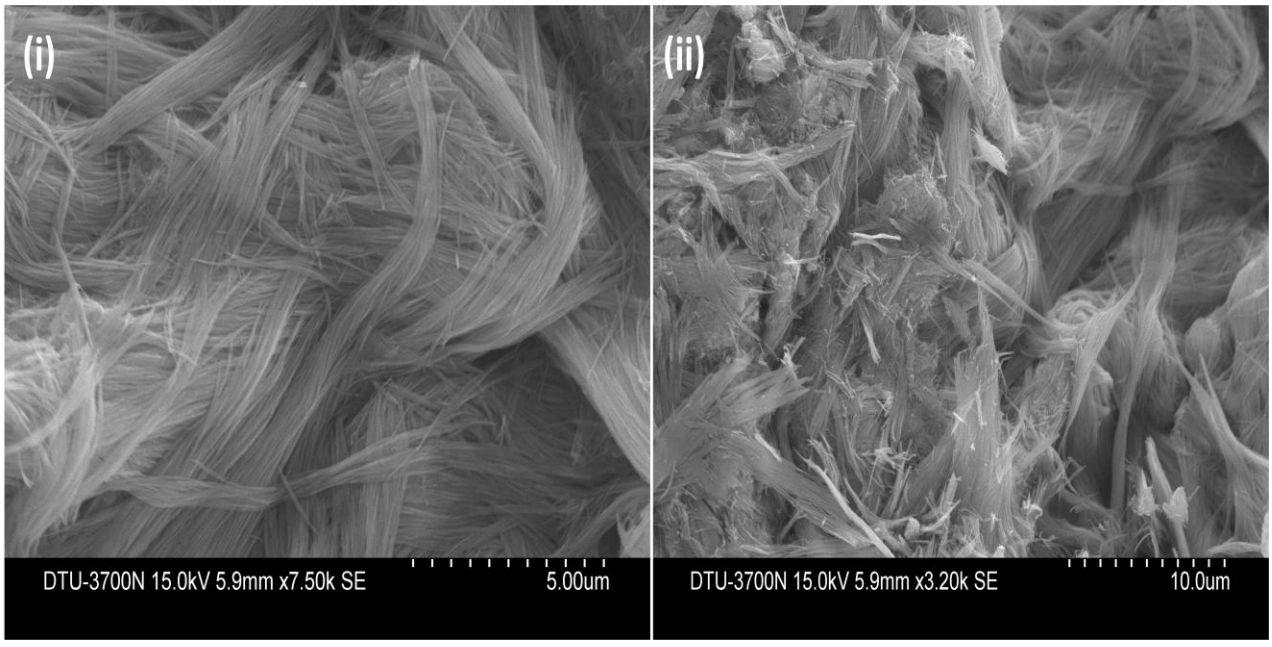

Fig 6.1 Scanning Electron microscope Image of Sample (d) having CuO nanowires (i) lower resolution (ii) Higher resolution

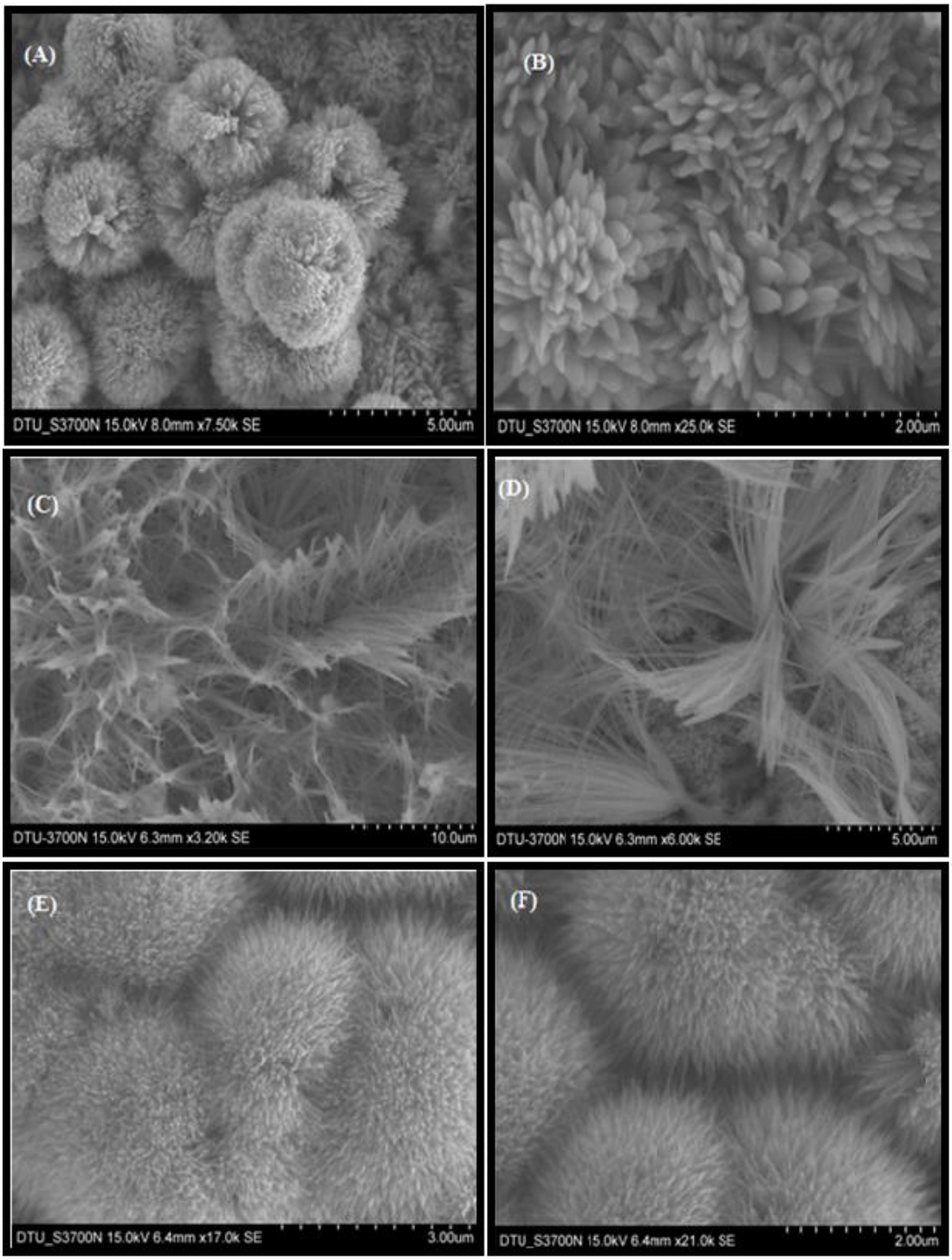

Fig.6.2. Scanning electron microscope images (a), (b) Samples at 11pH reaction time 96h (c), (d) samples at 11.5 pH reaction time 96h (e), (f) samples at 12pH reaction time 96h.

6.1.2 Energy-dispersive X-ray spectroscopy (EDX)

Fig 6.3 represents EDX spectra of prepared sample b (CuO nanorods) containing mainly Copper (Cu) and Oxygen (O). The as-deposited samples contain approx. 89 percent Cu & 11 percent O by weight.

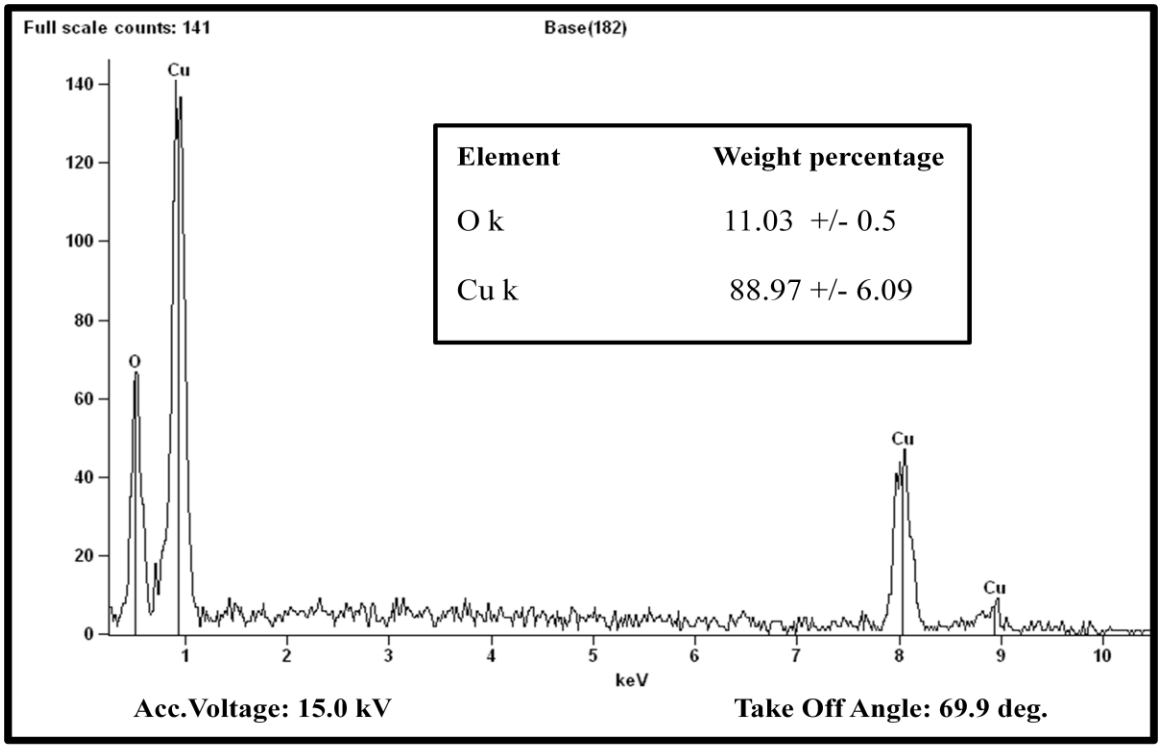

Fig 6.3 Energy dispersive X-Ray spectroscopy of CuO sample

6.1.3 X-ray diffraction (XRD)

Fig. 6.4 shows XRD of sample (a) (nanoflowers), sample (b) (nanorods) and sample (c) (dense nanorods). The XRD peaks seen at 35.5^0 corresponds to $(\bar{1}11)$ and (002) plane of CuO, whereas peak at 38.8^0 belongs to (111) & (200) planes of CuO (JCPDS-89-5895). These set of planes suggest that CuO system has monoclinic structure having end centered lattice. The lattice parameters of above system are a=4.682 Å, b=3.424 Å, c=5.127 Å. whereas the peaks arising at 43.2^0, 50.16^0 and 79.16^0 belongs to lattice planes (111), (200) and (220) of Cu foils, which has cubic structure with face centered lattice (JCPDS- 85-1326).

The average crystallite size of nanostructured CuO have been estimated using Debye-Scherrer equation,

$$\tau = \frac{K\lambda}{\beta \cos(\theta)}$$

The average crystallite size obtained for the following results are interpreted. The average crystallite size of CuO nanoflowers [sample (a)] as suggested by XRD data is found to be 16.83 nm. Whereas average Crystallite size of nanorods [sample (b)] is found to be 15.35 nm and average crystallite size of 13.71 nm has been found in sample (c). Thus it can be seen from the XRD results that crystallite size reduces on increasing the pH value of solution. This is represented in Fig 6.5.

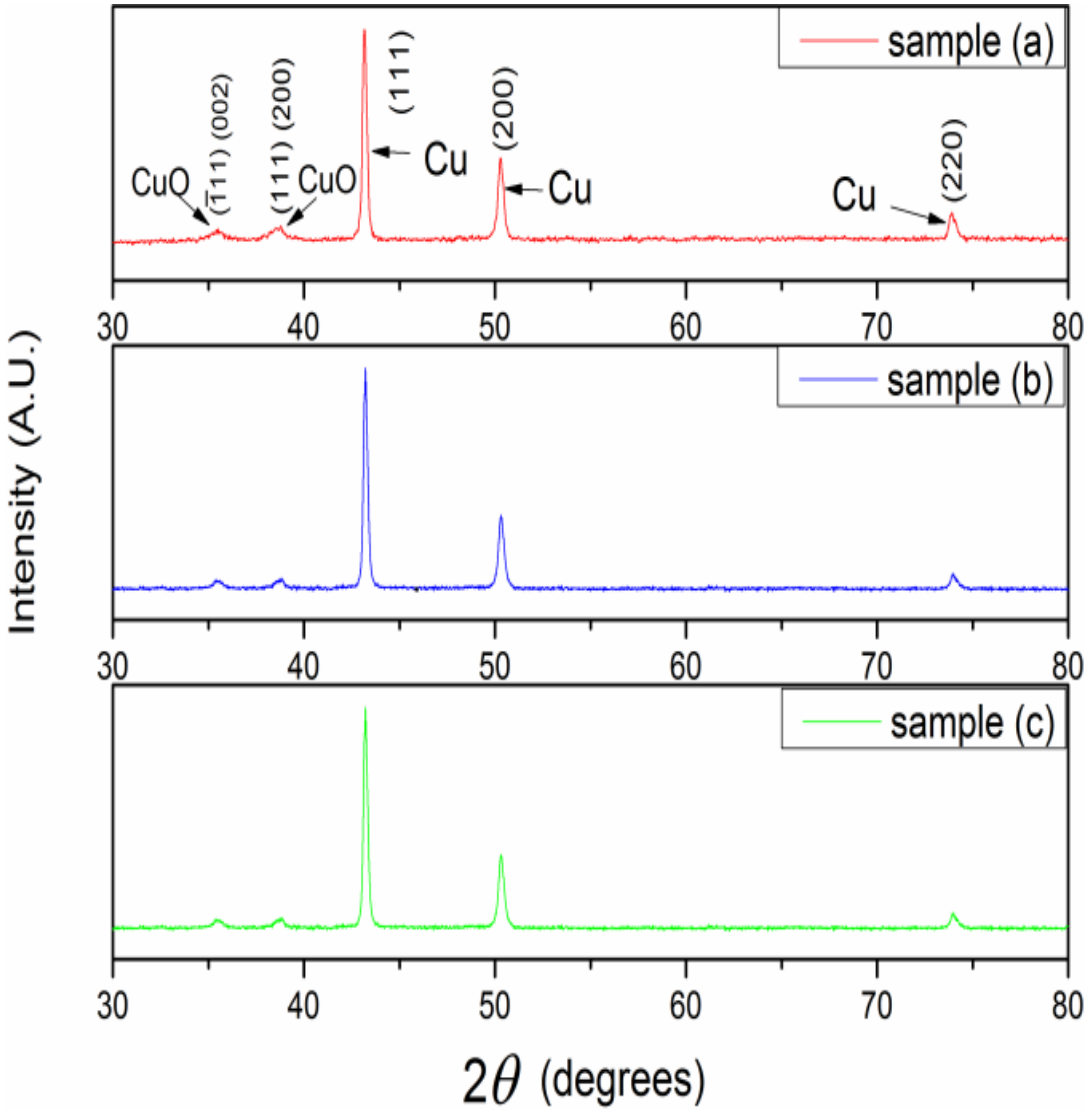

Fig.6.4 X-Ray diffraction pattern of nanostructured CuO sample (a), (b) and (c)

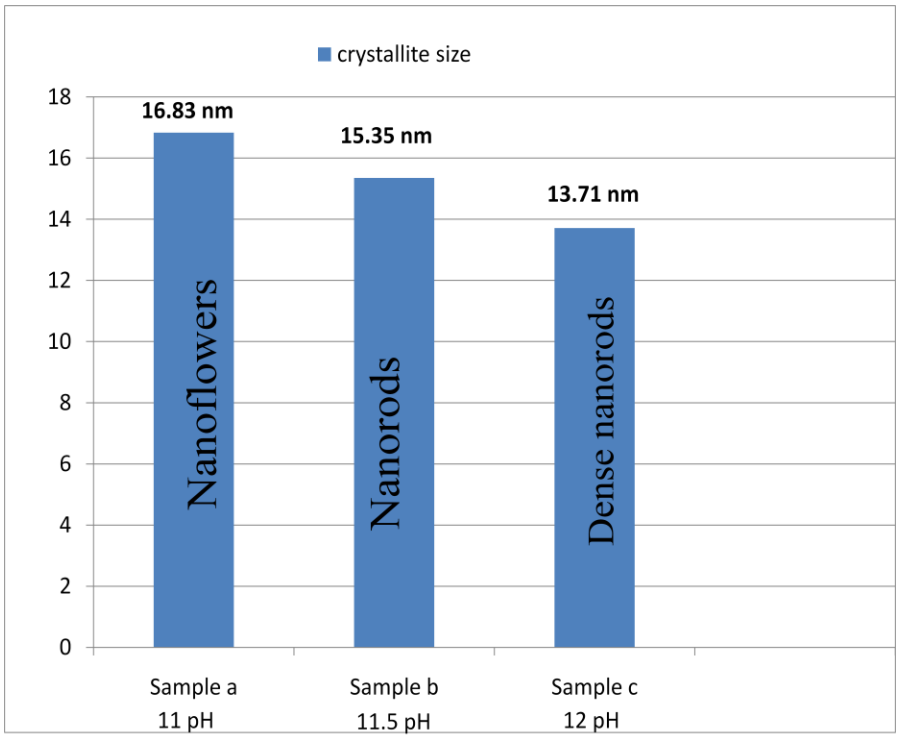

Fig 6.5 Graph representation of crystallite size against increasing pH of solution

We observe and deduce the affect of growth modifiers on crystallite size and morphological changes. Here OH^- ions act as growth modifiers which alter the shape and size of crystals as they grow, thus providing chemical control of crystal morphology. This growth modification of crystals can be explained by anisotropic face-specific growth kinetics. According to this crystal faces are discrete and having different kinetics for their growth depending on growth modifiers. These differences determine the shape and size of crystals. As pH increases, concentration of OH^- ions and density of CuO nanostructures increase. These compact structures result in reduced face-specific growth kinetics and crystallite size. This effect of pH on crystallite size is illustrated in **fig 6.5 [67]**.

6.1.4 Fourier Transform Infrared Spectroscopy (FTIR)

Fig 6.6 represents Fourier transform infrared (FTIR) spectra of CuO nanostructures sample (a), (b) and (c) in the range of 4000 cm^{-1} to 450 cm^{-1}. The characteristic bands observed at 509.9, 605.6 cm^{-1} and 422.8 cm^{-1} range can be assigned to metal oxide bonding which is Cu-O stretching **[68]**. The absorption bands between 1300 and 3500 cm^{-1} originates due to the

chemisorbed and/or physiosorbed H_2O and CO_2 molecules on the surface of CuO crystals. First peak at 3450.7cm^{-1} represent O-H stretch bonding of alcoholic group due to water molecule.

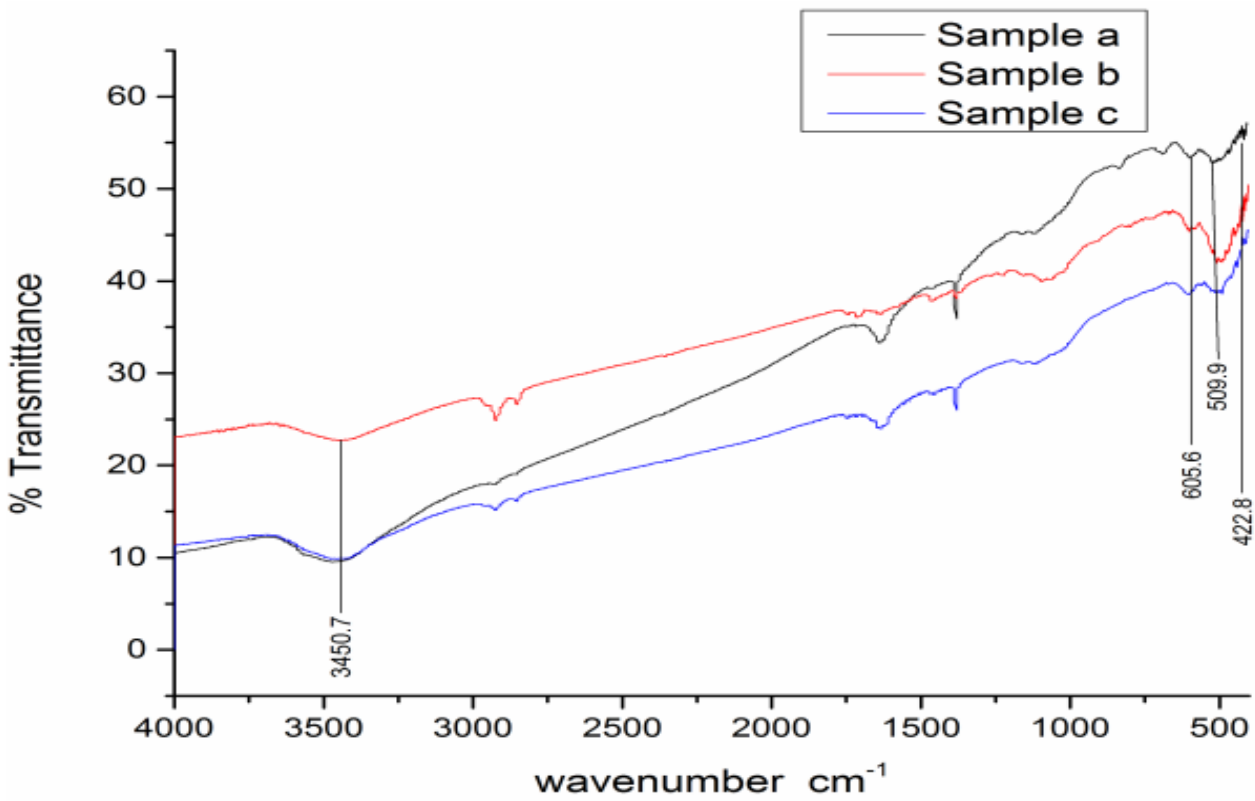

Fig 6.6 Fourier transform infrared spectrum of CuO sample (a), (b) and (c)

6.1.5 Transmission Electron Microscope (TEM)

Further TEM analysis of CuO nanorod [sample (b)] indicates the formation of nanorods having diameter in the range of 16.4 – 32.9 nm as shown in **Fig 6.7(a)**. **Fig 6.7(b)** shows selected area electron diffraction (SAED) pattern of CuO nanorods which conforms crystalline formation of nanorods. Different circles denote different miller planes of the nanostructure as supported by XRD studies.

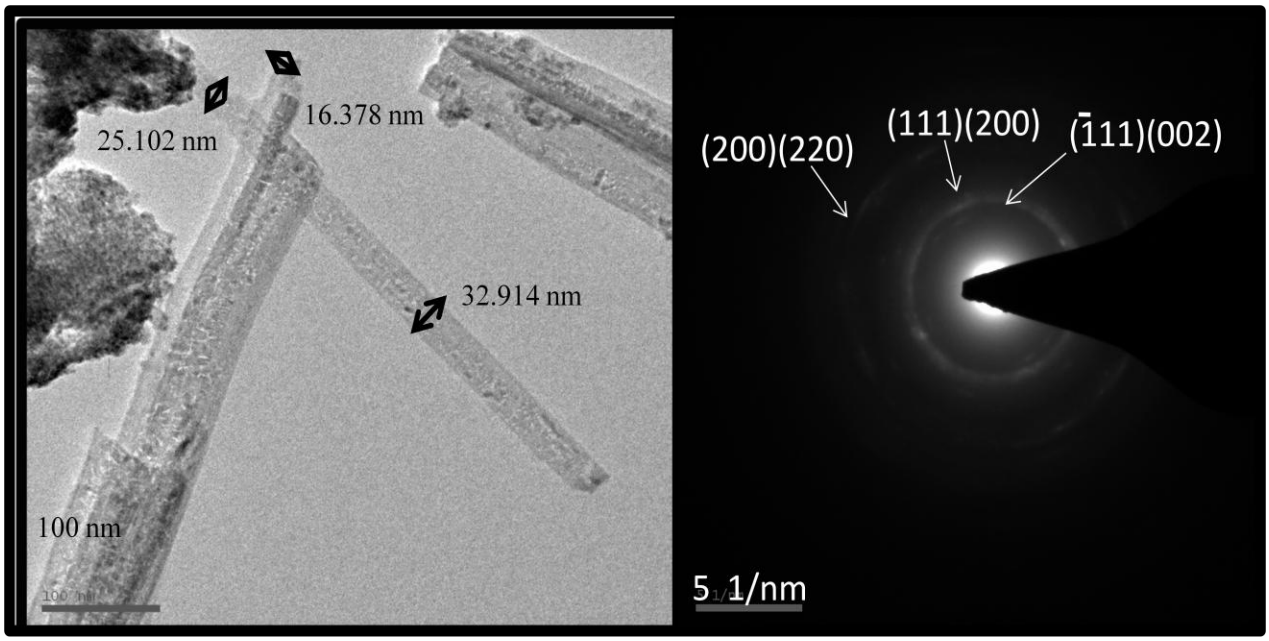

Fig 6.7 (a) TEM image (b) SAED pattern of CuO nanorod sample (b)

Chapter 7

7.1 Conclusions

In summary, we have successfully synthesized CuO nanostructures that are approximately 25 nm in diameter and several nm in length by a simple wet chemical method on copper foil. This method includes many advantages like low temperature, cost effective method and uniform size of nanostructures. Our method relies on the coordination self-assembly of the square planar complexes of Cu^{2+} which has been discussed in growth mechanism. We also have studied the effect of the solution pH on CuO nanostructures growth. It shows that higher pH value corresponds to good quality nanorods as compared to low pH value and the density of nanorods increases on increasing the pH value. With the help of XRD characterization we have deduced that crystallite size decreases on increasing concentration of growth modifiers such as OH^- ions. These nanostructures promise many potential applications in sensors. On other hand we have synthesized CuO nanowires successfully by wet chemical method having different precursors of Cu. Nanowires are formed in powder form which are characterized by scanning electron microscope. Thus these CuO nanoarchitectures have been synthesized successfully and can be used in many applications like an active electrode material for Li-ion batteries, field emission [FE] emitters, heterogeneous catalysts, gas sensors, and solar cells fields.

References

[1] Rao C N R, Muller A, Cheetham A K (eds), Chemistry of Nanomaterials, 2004, Wiley-VCH, Weinheim.

[2] Rao C N R, Cheetham A K, J Mater. Chem., 2001, 11, 2887.

[3] Rao C N R, Cheetham A K, Materials Science at the Nanoscale, Nanomaterials Handbook, Gogotsi Y (ed.), Taylor & Francis Group, 2006, New York, p.2.

[4] B.K.H. Yen, N.E. Stott, K.F. Jensen, M.G. Bawendi, A continuous-flow microcapillary reactor for the preparation of a size series of CdSe nanocrystals, Advanced Materials 15 (2003) 1858–1862.

[5] Yamamoto, K.; Kasuga, T.; Nogami, M.; Electrochem. Solid-State Lett.**1999**, *2*, 595-596. DOI: 10.1149/1.1390917

[6] Anandan, S.; Wen, X.; Yang, S.; Materials Chemistry and Physics 93, **2005**, 35–40. DOI: 10.1016/j.matchemphys.2005.02.002

[7] Wang, C; Q Fu, X.; Xue, X.; G Wang, Y.; H Wang, T.; Nanotechnology 18, **2007**, 145506 DOI: 10.1088/0957-4484/18/14/145506

[8] Anandan, S.; Wen, X.; Yang, S.; Materials Chemistry and Physics 93, **2005**, 35–40. DOI: 10.1016/j.matchemphys.2005.02.002

[9] Chowdhuri, A.; Sharma, P.; Gupta, V.; Sreenivas, K.; Rao, K V.; J Appl Phys, **2002**, 92:2172-2180. DOI: 10.1063/1.1490154

[10] Bennici, S.; Gervasini, A.; Appl Catal B, **2006**, 62:336-344. DOI: 10.1016/j.apcatb.2005.09.001

[11] Ghosh, S.; Avasthi, D K.; Shah, P.; Ganesan, V.; Gupta, A.; Sarangi, D.; Bhattacharya, R.; Assmann, W.; Vacuum, **2000**, 57:377-385. DOI: 10.1016/s0042-207x(00)00151-2

[12] Hsieh, C T.; Chen, J M.; Lin, H H.; Shin, H C.; Appl Phys Lett, **2003**, 83:3383-3385 DOI: 10.1063/1.1619229

[13] Switzer, J A.; Kothari, H M.; Poizot, P.; Nakanishi, S.; Bohannan, E W.; Chem. Mater., **2004**, 16 (22), pp 4232– 4244 DOI: 10.1021/cm048939x

[14] Martin, C.R.; Science 266, **1994**, 1961.
DOI: 10.1126/science.266.5193.1961

[15] Wang, Y D.; Ma, C L.; Sun, X D.; Li, X D.; Inorg. Chem. Commun. 5, **2002**, 751.
DOI: 10.1016/s1387-7003(02)00546-4

[16] Shi, W S.; Zheng, Y F.; Wang, N.; Lee, C S.; Lee, S T.; Adv. Mater. 13, **2001**, 591.
DOI: 10.1002/1521-4095(200104)13

[17] Pan, Z.W. ; Dai, Z.R.; Wang, Z.L.; Science 291, **2001**, 1947.
DOI: 10.1126/science.1058120

[18] Liu, S.W.; Yue, J.; Gedanken, A.; Adv. Mater. 13, **2001**, 656.
DOI: 10.1002/1521-4095(200105)13

[19] Morales, A.M.; Lieber, C.M.; Science 279, **1998**,208.
DOI: 10.1126/science.279.5348.208

[20] Ethiraj, A.S.; Kang, D.J.; Nanoscale Research Letters, **2012**, 7:70.
DOI: 10.1186/1556-276x-7-70

[23] http://enwikipediaorg/wiki/Copper(II)_oxide Access date 02/20/2012.

[24] Madelung O. Semiconductors : data handbook. Berlin ; New York: Springer; 2004.

[25] Arregui FJ. Sensors Based on Nanostructured Materials. Berlin: Springer US;
2008.

[26] Ghijsen J, Tjeng LH, Vanelp J, Eskes H, Westerink J, Sawatzky GA, et al. Electronic-Structure of Cu2o and Cuo. Phys Rev B. 1988;38:11322-30.

[27] Singh DP, Srivastava ON. Synthesis and Optical Properties of Different CuO (Ellipsoid, Ribbon and Sheet Like) Nanostructures. J Nanosci Nanotechno. 2009;9:5345-50.

[28] Berger LI. Semiconductor materials. Boca Raton, Fla. [u.a.]: CRC Press; 1997.

[29] A new lithium-ion battery: CuO nanorod array anode versus spinel $LiNi_{0.5}Mn_{1.5}O_4$ cathode Weixin Zhang, Guo Ma, Heyun Gu, Zeheng Yang, He Cheng

[30] Room temperature growth of CuO nanorod arrays on copper and their application as a cathode in dye-sensitized solar cells Sambandam Anandan, Xiaogang Wen, Shihe Yang

[31] Gas sensing properties of CuO nanorods synthesized by a microwave-assisted hydrothermal method Chao Yang, Xintai Su, Feng Xiao, Jikang Jian, Jide Wang

[32] Wide Linear-Range Detecting Nonenzymatic Glucose Biosensor Based on CuO Nanoparticles Inkjet-Printed on Electrodes Rafiq Ahmad, Mohammad Vaseem, Nirmalya Tripathy and Yoon-Bong Hahn.

[33] A. Pendashteh, M. S. Rahmanifar and M. F. Mousavi: 'Morphologically controlled preparation of CuO nanostructures under ultrasound irradiation and their evaluation as pseudocapacitor materials', Ultrason. Sonochem., 2014, 21, 643–652.

[34] Field emission properties of one-dimensional single CuO nanoneedle by in situ microscopy Yueli Liu Lei Zhong Zhuoyin Peng Yanbao Song Wen Chen.

[35] Synthesis of CuO Nanocrystals and Sequential Assembly of Nanostructures with Shape-Dependent Optical Absorption upon Laser Ablation in Liquid. X. Z. Lin, P. Liu, J. M. Yu, and G. W. Yang.

[36] Kingon, A. I.; Maria, J.-P.; Streiffer, S. K. Nature 2000, 406, 1032–1038.

[37] J. Z. Sun and A. Gupta, "Spin-Dependent Transport and Low-Field Magnetoresistance in Doped Manganites," Annu. Rev. Mater. Sci., vol. 28, pp. 45–78, 1998.

[38] C. N. R. Rao, A. Muller, and A. K. Cheetham, Eds., The chemistry of nanomaterials: Synthesis, Properties and Applications, vol. 1. Weinheim, Germany: WILEY-VCH Verlag GmbH & Co. KGaA, 2004.

[39] P. Barquinha, R. Martins, L. Pereira, and E. Fortunato, Transparent Oxide Electronics. Chichester, UK: John Wiley & Sons, Ltd, 2012.

[40] S. Djoki, Ed., Electrodeposition and Surface Finishing. New York, USA: Springer, 2014.

[41] C. Wang, L. Yin, L. Zhang, D. Xiang, and R. Gao, "Metal oxide gas sensors: Sensitivity and influencing factors," Sensors, vol. 10, pp. 2088–2106, 2010.

[42] "IUPAC Periodic Table of the Elements," 2013. [Online]. Available: http://www.iupac.org/fileadmin/user_upload/news/IUPAC_Periodic_Table-1May13.pdf. [Accessed: 12-Feb-2015].

[43] Synthesis of copper/copper oxide nanoparticles by solution plasma Genki Saito, Sou Hosokai, Masakatsu Tsubota, and Tomohiro Akiyamaa

[44] WILLEY-VCH Verlag GmbH & Co. KGaA, Weinheim ISBN : 3-527–30507–6.

[45] Formation of Uniform CuO Nanorods by Spontaneous Aggregation: Selective Synthesis of CuO, Cu2O, and Cu Nanoparticles by a Solid-Liquid Phase Arc Discharge Process. Wei-Tang Yao, Shu-Hong Yu, Yong Zhou, Jun Jiang, Qing-Song Wu, Lin Zhang, and Jie Jiang

[46] Synthesis of large-area and aligned copper oxide nanowires from copper thin film on silicon substrate. Kaili Zhang, Carole Rossi, Christophe Tenailleau, Pierre Alphonse and Jean-Yves Chane-Ching.

[47] Preparation of CuO nanostructures coating on copper as supercapacitor materials. M. M. Momeni, Z. Nazari, A. Kazempour, M. Hakimiyan and S. M. Mirhoseini.

[48] Controlled synthesis of highly ordered CuO nanowire arrays by template-based sol-gel route. SU Yi-kun, SHEN Cheng-min**,** ANG Hai-tao, LI Hlin, A O Hong-jun.

[49] Room temperature growth of CuO nanorod arrays on copper and their application as a cathode in dye-sensitized solar cells. Sambandam Anandan, Xiaogang Wen, Shihe Yang.

[50] Gas sensing properties of CuO nanorods synthesized by a microwave-assisted hydrothermal method. Chao Yanga, Xintai Sua, Feng Xiaoa, Jikang Jian, Jide Wanga.

[51] Synthesis and characterization of CuO nanowires by a simple wet chemical method. Anita Sagadevan Ethiraj and Dae Joon Kang.

[52] Synthesis of hierarchical CuO microspheres: Photocatalytic and antibacterial activities. R. Sathyamoorthy, K.Mageshwari.

[53] Sathyamoorthy, R.; Mageshwari, K.; Physica E, **2013**, 47E, 157–161.
DOI: 10.1016/j.physe.2012.10.019

[54] Dara, M.A.; Ahsanulhaq, Q.; Kim, Y.S.; Sohn, J.M.; Kim, W.B.; Shin, H.S.; Applied Surface Science 255, **2009**, 6279–6284.
DOI: 10.1016/j.apsusc.2009.02.002

[55] Dayeh, S. A.; Yu, E. T.; Wang, D.; Nano letters, **2007**, Vol. 7, No. 8 2486-2490.
DOI: 10.1021/nl0712668

[56] Wen, X.; Zhang, W.; Yang, S.; Langmuir **2003,** 19, 5898-5903.
DOI: 10.1021/la0342870

[57] Wen, X.; Zhang, W.; Yang, S.; Nano letters, **2002**, Vol. 2, No. 12 1397-1401.
DOI: 10.1021/nl025848

[58] UhlandWeissker, Silke Hampel, Albrecht Leonhardt and Bernd B¨uchner, Carbon Nanotubes Filled with Ferromagnetic Materials.

[59] UhlandWeissker, Silke Hampel, Albrecht Leonhardt and Bernd B¨uchner, Carbon Nanotubes Filled with Ferromagnetic Materials.

[60] UhlandWeissker, Silke Hampel, Albrecht Leonhardt and Bernd B¨uchner, Carbon Nanotubes Filled with Ferromagnetic Materials.

[61] Https://en.wikipedia.org/wiki/X-ray_crystallography

[62] Https://en.wikipedia.org/wiki/Scanning_electron_microscope

[63] Nanotechnology:Practices and principle by sulebha kulakarni.

[64] Https://en.wikipedia.org/wiki/Raman_spectroscopy.

[65] Nanotechnology:Practices and principle by sulebha kulakarni.

[66] Nanotechnology:Practices and principle by sulebha kulakarni.

[67] Garcia, S.P.; Semancik, S.; Chem. Mater. **2007**, 19, 4016-402 DOI: 10.1021/cm061977r.

[68] Koji, N.; Infrared Absorption Spectroscopy, QD95.N383. DOI: 10.1002/jps.2600520742.

Notes